Multisensory integration of social signals by a pathway from the basal amygdala to the auditory cortex in maternal mice

Alexandra C. Nowlan, Clancy Kelahan, and Stephen D. Shea*

Cold Spring Harbor Laboratory
1 Bungtown Road
Cold Spring Harbor, New York 11724, USA

***Corresponding author**:

Phone: (516) 367-8823
Fax: (516) 367-8453
email: sshea@cshl.edu

Acknowledgements: The authors wish to thank J. Sturgill and J. Choe for technical assistance, the Zador, Tollkuhn and Li laboratories for their contributions, and Shea Lab members for helpful comments and discussion. Figures 1A-B, 3A-B, and 5A were created using Biorender.com. This work was supported by a grant to SDS from the National Institute of Mental Health (R01MH119250) and a grant to SDS from the C.M. Robertson Foundation

ABSTRACT

Social encounters are inherently multimodal events, yet how and where social cues of distinct modalities merge and interact in the brain is poorly understood. For example, when their pups wander away from the nest, mother mice use a combination of vocal and olfactory signals emitted by the pups to locate and retrieve them. Previous work revealed the emergence of multisensory interactions in the auditory cortex (AC) of both dams and virgins who co-habitate with pups ('surrogates'). Here we identify a neural pathway that integrates information about odors with responses to sound. We found that a scattered population of glutamatergic neurons in the basal amygdala (BA) projects to the AC and responds to odors, including the smell of pups. These neurons also exhibit increased activity when the surrogate female is searching for pups. Finally, we show that selective optogenetic activation of BA-AC neurons modulates responses to pup calls, and that this modulation switches from predominantly suppressive to predominantly excitatory after maternal experience. This supports an underappreciated role for the amygdala in directly shaping sensory representations in an experience-dependent manner. We propose that the BA-AC pathway integrates olfaction and audition to facilitate maternal care, and speculate that it may carry valence information to the AC.

INTRODUCTION

In sharp contrast to how most sensory neurophysiology and psychophysical research has historically been conducted, organisms engaged in unstructured natural behavior typically make decisions by considering all sensory data available to them. For example, during social encounters, individuals are often informed about the identity and status of conspecifics by interpreting a combination of auditory, olfactory, tactile, and/or visual cues. While the significance of all these modalities have individually been well-studied, much less is known about how qualitatively distinct pieces of social information from different senses are integrated in the brain to guide behavior. Here we examine the neural circuitry that underlies multisensory integration of odor and sound during natural maternal behavior in mice.

Shortly after giving birth, first time mother mice learn to respond to ultrasonic vocalizations (USVs or 'calls'), emitted by pups when they are separated from the litter, by locating them and bringing them back to the nest ('pup retrieval') (Ehret et al., 1987; Miranda and Liu, 2009). Sensory experience with pups is sufficient to motivate pup retrieval because virgin females co-housed with pups ('surrogates') also learn to retrieve without the influence of pregnancy hormones (Rosenblatt, 1967; Galindo-Leon et al., 2009; Cohen et al., 2011; Cohen and Mizrahi, 2015; Stolzenberg and Champagne, 2016; Krishnan et al., 2017; Lau et al., 2020; Carcea et al., 2021). Consistent with the importance of USV detection for pup retrieval, activity and plasticity of the auditory cortex (AC) is implicated in accurate and efficient pup retrieval (Galindo-Leon et al., 2009; Cohen et al., 2011; Cohen and Mizrahi, 2015; Krishnan et al., 2017; Lau et al., 2020). Audition and olfaction are jointly required because disrupting olfactory processing also interferes with retrieval (Cohen et al., 2011; Wang and Storm, 2011; Weiss et al., 2011; Fraser and Shah, 2014). Interestingly, there is evidence that separate signals related to odor and sound may

merge in the AC. Delivery of pup odors to anesthetized female mice acutely modulates single neuron AC responses to a range of sounds including USVs, but only in pup-experienced females (mothers and surrogates), not naïve females (Cohen et al., 2011; Cohen and Mizrahi, 2015). The brain pathway by which odor information reaches the AC is unknown.

We took advantage of the ability of virgin females to learn pup retrieval in order to study the neural circuit that integrates odor signals in the AC. This allowed us to observe the effects of sensory experience on this pathway independent of pregnancy hormones. We report the following findings. First, we used anatomical tracing to identify a population of neurons in the basal amygdala (BA) that project into the AC. Second, we used an intersectional viral strategy to label the AC projecting BA neurons (BA-AC) with the calcium (Ca^{2+}) sensor GCaMP6s. Fiber photometry in awake, head-fixed mice revealed that BA-AC neurons respond to odor, including the smell of pups. Third, we performed fiber photometry in freely behaving mice and found that their activity is elevated during active search for pups. Finally, we optogenetically activated BA-AC neurons in anesthetized females and found that activation modulates responses to sound. This modulation switches from predominantly suppressive to predominantly excitatory after maternal experience. Based on these observations, we propose that neurons in the BA carry odor information to the AC, where they influence auditory activity to improve pup retrieval. This contrasts with other forms of multisensory integration in the auditory cortex that emerge via inputs from primary sensory structures. Moreover, our results reveal an underappreciated role for the amygdala in directly modulating sensory representations in accordance with maternal status.

RESULTS

Olfaction is required for pup retrieval behavior in surrogate females

Nulliparous female mice that have sustained exposure to pups, e.g. via co-habitation with a mother and her litter, learn to perform efficient pup retrieval within a few days (Rosenblatt, 1967; Stolzenberg and Champagne, 2016). Previous reports regarding the influence of pup odors on auditory activity in the AC found evidence of this integration in both mothers and surrogates. Here we took advantage of this property by performing all experiments reported here in surrogates to simplify controlling their experience with pups independent of pregnancy.

The necessity of olfactory signals for maternal behavior in dams has already been established (Cohen et al., 2011; Wang and Storm, 2011; Weiss et al., 2011; Fraser and Shah, 2014), however it is unknown whether surrogates share this requirement. Thus, we performed behavioral experiments to test the importance of odor cues for retrieval in surrogates. We assayed the pup retrieval performance of naïve virgin females beginning prior to co-habitation with a pregnant dam and continuing throughout their surrogacy on postnatal day 0, 3, and 5 (Figure 1A, B). Performance was quantified using a normalized measure of latency to retrieve ('latency index'; see Materials and Methods) (Krishnan et al., 2017). Then, we used the tissue specific toxicant methimazole (MMZ) to ablate the olfactory epithelium of these mice and again measured their retrieval performance after the ablation was complete (Figure 1F). As expected, naïve virgins exhibited poor pup retrieval (naïve latency index: 0.622 ± 0.09; all values are reported as mean ± SEM unless otherwise noted). The same mice were each subsequently paired with a pregnant dam as surrogates, and they exhibited a significant decrease in retrieval latency by P3 (P3 latency index: 0.060 ± 0.01; Tukey's multiple comparisons test; $p = 0.023$) and P5 (P5 latency index: 0.052 ± 0.01; Tukey's multiple comparisons test; $p = 0.017$) compared to their naïve performance (Figure 1C). After MMZ treatment, retrieval latency substantially increased (MMZ latency: 0.872 ± 0.08) and did not significantly differ from the latency of naïve mice (Tukey's multiple comparisons test; $p = 0.249$).

Moreover, the percentage of pups retrieved significantly decreased from 100% for all subjects on P5 to 13.33% ± 0.08 after ablation of the MOE (Figure 1D; Tukey's multiple comparisons test, $p = 0.002$). These data are consistent with a requirement for volatile odor detection via the main olfactory epithelium for pup retrieval in surrogates.

Because MMZ injection took 3-7 days to achieve full effect, we had to replace the co-housed pups that had grown too large for retrieval with a younger litter. Therefore, we confirmed that the impaired retrieval performance was due to diminished olfactory function rather than introduction of a litter of unfamiliar pups. We measured retrieval performance of the surrogates using a novel litter of pups before treatment with MMZ. The latency to retrieve novel pups and the latency to retrieve the familiar pups with which they had been co-housed did not significantly differ (Figure 1E; Wilcoxon matched-pairs signed rank test, $p = 0.625$). Based on these results, we conclude that the retrieval responses shown by surrogates are not exclusive to the pups to which they were first exposed. Moreover, the poor retrieval exhibited by MMZ-treated surrogates was not related to gathering an unfamiliar litter, but can be attributed to disrupted olfactory signaling.

Projection neurons within the BA target the AC

Despite prior reports that pup odor can dramatically influence responses to auditory stimuli in the AC, the pathway by which odor signals reach the AC is unknown. We therefore used retrograde viral tracing methods to identify candidate inputs to the AC that could carry odor information and modulate auditory activity. We injected AAVrg-CAG-tdTomato (tDT) into the left AC as a retrograde neuronal tracer to label brain areas that project to the AC (Figure 2 A-D). In addition to known AC afferent structures such as the contralateral AC, the medial geniculate body of the thalamus (MGB), and the piriform cortex (Figure 2 C-D), we observed tdT-labeled

cells in both the ipsi- and contralateral basolateral and basomedial amygdala. Henceforth, we collectively refer to these as the basal amygdala (BA, Figure 2A). Neurons in the BA constitute an important component of the circuitry that governs maternal behavior. They receive multimodal sensory input, including olfactory input (Okabe et al., 2013), and are proposed to contribute to appetitive maternal responses by conveying sensory information to the mesolimbic reward system (Petrovich et al., 1996; Perry and McNally, 2013). In rats, inactivation of the BA selectively disrupts pup retrieval behavior, without affecting other maternal behaviors, like nursing (Numan et al., 2010), suggesting that BA participates in goal-directed aspects of maternal care. Moreover, neurons in the BA receives input from neighboring olfactory amygdala nuclei (Canteras et al., 1995). Based on these properties, we chose to more closely examine the population of BA neurons that project to the AC.

To quantify the extent of the BA-AC projection, we performed separate tracing experiments injecting AAVrg-hSyn-Cre-WPRE-hGH virus into the AC of Rosa26-stop^{flox}-H2B-GFP mice. With this strategy, Cre activated a nuclear-localized GFP in retrogradely labeled neurons, facilitating automated cell counting. Thousands of neurons (Figure 2E; 4513 ± 1977 cells; n = 3 mice) were labeled throughout the BA. To learn more about the neurochemical identity of the neurons that contribute to the BA-AC pathway, we performed additional retrograde tracing experiments in several lines of transgenic mice that express Cre in different populations of glutamatergic or GABAergic neurons (Slc17a7$^{tm1.1(cre)Hze}$/J, vesicular glutamate transporter type 1 (vGlut1); Slc17a6$^{tm2(cre)Lowl}$/J, vGlut2; or Slc32a1$^{tm2(cre)Lowl}$/J, vesicular GABA transporter (vGAT)). Not surprisingly, injections of AAV that was Cre-independent labelled the largest number of cells in the BA-AC projection neurons (Figure 2G). Injections of AAV driving Cre-dependent expression of fluorophore, AAVrg-FLEX-tdTomato resulted in less extensive labeling

overall, but only in VGlut1-Cre and VGlut2-Cre mice (Figure 2F; VGlut1-Cre: 380.3 ± 23.99 neurons, n = 3 mice; VGlut2-Cre: 256.3 ± 43.17 neurons, n = 6 mice). No retrogradely-labelled neurons were found in VGAT-Cre mice (n = 3 mice). Based on our viral retrograde tracing experiments, we conclude that a relatively large, but heterogeneous population of glutamatergic excitatory neurons in the BA project to the AC (Figure 2G).

BA-AC projection neurons respond to odors including pup odor

To determine whether the BA-AC projection neurons were sensitive to pup-related odors, we used fiber photometry in awake head-fixed mice to measure bulk Ca^{2+}signals from BA-AC neurons in response to olfactory stimuli. We selectively labelled the BA-AC projection neurons by using the intersectional viral strategy depicted in Figure 3A (see also Figure 3 – figure supplement 1). Briefly, we injected retrograde AAVrg-hSyn-Cre-WPRE-hGH into the AC and made an injection of AAV5-syn-FLEX-GCaMP6s-WPRE into the BA, thereby expressing the fluorescent Ca^{2+} sensor GCaMP6 exclusively in BA neurons that project to the AC. After 3 weeks to allow for viral expression, naïve virgin females were habituated for several days to head fixation on a wheel and then presented with pseudorandomized 2 s trials of monomolecular odorants or pup odor and clean nesting material every 30 s (Figure 3B).

We observed robust, odor-evoked changes in fluorescence in response to monomolecular odors (Figure 3C-E). Most odors in most mice elicited an abrupt increase in GCaMP fluorescence within 1 s and lasting about 3 s (Figure 3D). The magnitude of Ca^{2+} signals was variable depending on the individual subject and the odor presented (Figure 3 – figure supplement 2). Comparing the stimulus-evoked signal to baseline for all mice (n = 8), mean Ca^{2+} fluorescence showed a significant increase for each of four monomolecular odors presented (Figure 3E; Wilcoxon signed

rank test, $p < 0.01$). We confirmed that the responses to these stimuli were mediated by the main olfactory system by comparing them to responses in a subset of mice after ablating their main olfactory epithelia with injection of MMZ. Subsequent to ablation, we no longer observed significant responses to any of the monomolecular odors (Figure 3C, F; Wilcoxon signed rank test, $p \geq 0.05$, n = 5 mice).

In addition to these arbitrary, non-social odors, we presented pup odor by collecting the headspace of a glass jar containing several pups (age 2 – 4 days) and directing the stream of odorized air onto the nose of a head-fixed, fiber-implanted mouse. In virgin females without maternal experience, we observed a clear increase in Ca^{2+} signal in response to pup odor that had a similar temporal structure to the responses to non-social odors (Figure 3G, 0.634 ± 0.25 z-dFF; Wilcoxon signed rank test, $p = 0.031$, n = 6 mice). As seen with other odors, this response was abolished after MMZ treatment (0.163 ± 0.09 z-dFF; Wilcoxon signed rank test, $p = 0.188$, n = 5 mice). Interestingly, in contrast to responses to non-social odors, responses to pup odor were not detected in mice that had completed five days of surrogacy (Figure 3H, 0.080 ± 0.17, Wilcoxon signed rank test, $p = 0.688$, n = 6 mice). The decreased calcium responses in surrogates were not due to a general insensitivity to odor, as significant responses to nesting materials persisted (Figure 3H; 0.432 ± 0.05, Wilcoxon signed rank test, $p = 0.031$). No odor evoked changes in fluorescence were observed in control animals injected to express GFP in BA-AC neurons instead of GCaMP (Figure 3 – figure supplement 3A; paired t-test comparing z-dFF at baseline (2 s) to after odor delivery (3 s), $p > 0.05$, Figure 3 – figure supplement 3B; Wilcoxon signed rank test, $p > 0.05$), verifying that the fluctuations we measured in response to odors reflect neural activity and not movement or other artifacts. Based on the above data, we conclude that the BA-AC projection

neurons respond to pup odor and therefore constitute a likely candidate pathway for odor information to access the AC.

BA-AC neurons are active during pup-seeking

Having discovered that BA-AC neurons were sensitive to pup odor, we next asked how they may participate in free interactions with pups, including retrieval. To do this, we recorded Ca^{2+} activity from BA-AC neurons in freely behaving females daily as they performed pup retrieval from the naïve state through surrogacy. Based on the results of the head-fixed experiments, we hypothesized that we would observe odor-evoked responses in the BA-AC neurons when a naïve female engaged with pups by picking them up or sniffing them during the retrieval behavior. Surprisingly, we observed by aligning the fluorescent traces to the mouse's behavior that while searching for pups (defined here as time between egress from the nest and either contact with a pup or returning to the nest), Ca^{2+} signals were elevated (Figure 4A). For a more systematic analysis, we segmented pup retrieval into four behavioral events: pup retrieval, pup sniffing, air sniffing and search. When GCaMP traces were aligned to each phase of retrieval, BA-AC neurons only showed a significant increase in activity as the females (n = 10 mice) searched the cage for a pup (Figure 4D; Wilcoxon signed rank test, $p = 0.027$), not when they made contact to retrieve or engaged with a pup physically by sniffing it. In fact, the fluorescent signal dropped significantly as soon as contact with a pup was made for retrieval (Figure 4B-D, Wilcoxon signed rank test, $p = 0.004$) or investigation (Figure 4D; Wilcoxon signed rank test, $p = 0.010$). These results suggest that the BA-AC circuit is primarily active during exploratory and/or goal-directed aspects of maternal behavior.

Optogenetic activation of BA-AC neurons bidirectionally modulates AC activity

Presenting pup odor acutely modifies auditory responses in the AC of female mice with maternal experience. Having established that the BA-AC projection neurons are responsive to pup odor, and are active during search for pups, we therefore hypothesized that selective optogenetic activation of the BA-AC pathway may modulate auditory responses in AC. We tested this hypothesis using an intersectional viral strategy to selectively label the BA-AC projection neurons with either the excitatory opsin, Channelrhodopsin-2 (ChR2), or GFP as a control (Figure 5A). After several weeks to allow for stable expression, mice in both groups were used for acutely anesthetized extracellular recording experiments. Auditory cortical neurons were recorded with the 'loose patch' technique (Cazakoff et al., 2014; Lau et al., 2020) while presenting a set of tones and pup vocalizations (calls) in pseudorandom order (see Materials and Methods). On 50% of trials, BA-AC axon terminals labelled with ChR2 were activated by directing blue light (473nm) onto the cortical surface (Figure 5B). To examine the effect of maternal experience, recordings were performed in either naïve virgins or surrogate mothers.

We recorded 83 neurons from 17 ChR2 injected mice (34 from 7 naïves and 49 from 10 surrogates) and 72 units from 15 GFP injected mice (33 from 7 naïve and 39 from 8 surrogates). All neurons exhibited stimulus-specific activity, and in ChR2-expressing mice, responses to some or all stimuli were modified by optogenetic activation. For example, on trials without light stimulation, the neuron depicted in Figure 5 B and C showed significant increases in firing to 16, 20, 25, and 32 kHz tones. However, on trials with light activation of the BA-AC terminals, responses to several tones were abolished (Figure 5B, lower panels and Figure 5C, blue trace). In

some neurons, stimuli that elicited no response on trials without optogenetic activation, actually did evoke a significant response on trials with light (Figure 5 D, E).

We quantified the magnitude and the prevalence of light modulation for all neurons and stimuli by performing a receiver operator characteristic (ROC) analysis for each cell-stimulus pair (see Materials and Methods). In this analysis, the area under the ROC curve (auROC) can be used as a measure of the discriminability between light-on versus light-off trials. We found that in naïve virgins, the auROC values for units recorded from ChR2 animals were significantly greater than those observed in GFP controls (Figure 5 F, G; ChR2: 0.623 ± 0.005; GFP: 0.574 ± 0.003, Mann-Whitney U-test, $p < 0.0001$). The same was true in surrogates (Figure 5 F, G, ChR2: 0.610 ± 0.005; GFP: 0.576 ± 0.003, Mann-Whitney U-test p = 0.0005). Therefore, the modulation of auditory responses was due to optogenetic activation and not light itself.

The direction of modulation was not accounted for in the above analysis, but it varied by neuron and stimulus. We observed examples of both optogenetic enhancement *and* suppression of auditory response strength in naïve females (Figure 5 B, E) and surrogates (Figure 5 – figure supplement 1). However, comparison of the effect of optogenetic activation of the BA-AC pathway revealed that maternal experience flipped the balance from predominantly suppression in naïve females (Figure 6A) to predominantly enhancement in surrogates (Figure 6B).

To determine whether stimulus frequency might influence this categorical outcome, we used Fisher's exact test to compare the number of units enhanced and suppressed by optogenetic stimulation from ChR2 injected animals versus GFP controls. For the majority of tones presented, the effect of optogenetic activation on AC responses to sound was independent of tone frequency (Figure 6 – figure supplement 1A). The only exception was naïve responses to 32kHz tones (Fisher's exact test, $p = 0.020$). Similarly, the effect of activation of the BA-AC pathway was

independent of the call exemplar presented, with the exception of surrogate responses to call exemplar 5 (Figure 6 – figure supplement 1B, Fisher's exact test, $p = 0.0003$).

To quantify the general predominance of optogenetic enhancement observed in surrogates, we calculated a modulation index (see Materials and Methods) to measure the change in response strength between light off and light on trials. We observed significant differences in modulation index between the naïve and surrogate animals for both tone stimuli (Figure 6C; naïve: n = 226 cell-stimulus pairs, -0.185 ± 0.037; surrogate: n = 291 cell-stimulus pairs, 0.031 ± 0.034; Mann-Whitney U test, $p < 0.0001$) and USVs (Figure 6C; naïve: n = 175 cell-stimulus pairs, -0.110 ± 0.042, surrogate: n = 274 cell-stimulus pairs, 0.055 ± 0.032; Mann-Whitney U test, $p = 0.0006$). There was no difference in the modulation index between naïve and surrogate GFP control mice for either tone or USV stimuli (Figure 6D; Mann-Whitney U test, $p \geq 0.05$). Similar to what we observed in the number of enhanced units, the distribution of modulation indices was independent of stimulus identity (Figure 6 - supplement 1 C,D; naïve, 2-way ANOVA, $p > 0.05$, n = 34 units, 7 mice; surrogates, 2-way ANOVA, $p > 0.05$, n = 46 units, 10 mice).

In some cases, we observed a change in firing rate on light only trials, during which no auditory stimulus was played (e.g. Figure 6E). While only some cells exhibited a change in firing on light only trials, considering all cells from ChR2-expressing mice, we found that light only responses were significantly more positive in surrogates as compared to the effect of optogenetic BA-AC activation in naïve mice (Figure 6F; naïve: n = 34 neurons, -0.091 ± 0.078; surrogates: n = 49 neurons, 0.237 ± 0.101, Mann-Whitney U test, $p = 0.025$). Again, we discovered a significant experience-dependent bias in the strength of the light only response. In naïve animals, ongoing activity was suppressed by activation of the BA-AC pathway, while in surrogates it was enhanced.

DISCUSSION

Like most social encounters, interactions between rodent pups and their parents are multisensory. They include somatosensory components and, most relevant to this work, auditory and olfactory components. The importance of pup vocalizations for eliciting retrieval is clear from several observations. First, dams will phonotax towards playback of natural USVs and synthetic USVs within the appropriate high-frequency range (Ehret and Haack, 1981). Second, pups that are congenitally mute are largely ignored by their mothers, even when they are separated from the nest (Hernandez-Miranda et al., 2017). Third, many studies have shown that initial maternal experience in both dams and virgin surrogates is correlated with plasticity in auditory responses in the auditory cortex (AC) (Galindo-Leon et al., 2009; Cohen et al., 2011; Cohen and Mizrahi, 2015; Krishnan et al., 2017; Lau et al., 2020). Finally, in our prior work on the impairment of maternal behavior in a mouse model of Rett syndrome (*Mecp2*^{het}), we showed that knocking out *Mecp2* only in the AC post-development was sufficient to substantially impair retrieval performance (Krishnan et al., 2017).

Although less well-studied, olfactory cues from the pups are also acknowledged to be essential for pup retrieval. For example, interfering with a mother's ability to detect volatile pup odors, either by genetically inactivating crucial components of olfactory signaling or by washing the pups to remove their odor, significantly diminishes retrieval performance (Cohen et al., 2011; Wang and Storm, 2011; Weiss et al., 2011; Fraser and Shah, 2014). Notably, here we confirmed and extended this finding to include virgin surrogates that had already established retrieval proficiency. By using the tissue-specific toxicant MMZ to ablate the main olfactory epithelium (MOE), we demonstrated that they almost completely lost the ability to gather pups. This raises several possibilities for the role olfactory cues play in maternal retrieval behavior: they may help

guide the female to the location of the pup, they may influence the perception of USVs, and/or they may trigger maternal experience-induced plasticity in the AC.

Despite the shared importance of USVs and pup odor for maternal care, relatively little is known about the circuits that coordinate audition and olfaction during maternal behavior. Previous work by Cohen and colleagues (Cohen et al., 2011; Cohen and Mizrahi, 2015) showed that the odor of pups directly interacts with AC responses to sounds, including USVs. Importantly, this interaction was only observed in mothers or surrogates with maternal experience. However, the circuit by which the pup odor accessed the AC was not identified.

Here we attempted to identify a specific neural pathway that could integrate the influence of odor with sensory representations of USVs in the AC. We began by injecting viral tracers into the AC to reveal candidate inputs. We identified the basal amygdala (BA) as a region that could carry information regarding odors due to its connections to olfactory areas of the amygdala (Canteras et al., 1995). We also observed sparse labeling of neurons in the piriform (olfactory) cortex. Nevertheless, in light of prior studies linking the BA with maternal behavior (see below), we instead chose to focus on its projection to the AC.

We made the following observations regarding the BA-AC pathway: First, we identified the BA neurons that project to the AC as likely predominantly glutamatergic. Second, with fiber photometric recordings exclusively from BA neurons that project to the AC, we demonstrated that these neurons robustly respond to pup odor and other odors more broadly. Interestingly, responses to pup odor disappeared or weakened in mice with several days of maternal experience. Third, we found that BA-AC neurons are active in freely behaving surrogates, particularly while the mouse is searching for pups, and rapidly become less active when she contacts them. Fourth, we found that optogenetic activation of the terminals of BA-AC changed the response of AC neurons to

sound, sometimes dramatically. Finally, in naïve virgins, activation predominantly led to inhibition of auditory responses, while in surrogate mice, activation predominantly led to excitation. We conclude that a glutamatergic projection from the basal amygdala regulates auditory cortical activity in an experience-dependent manner during pup interactions, in part driven by odors.

Implications for the auditory cortex

The pathway from the BA to the AC has not been widely studied. Responses to sound in AC are modulated by emotionally-charged stimuli (Chavez et al., 2009; David et al., 2012; Chavez et al., 2013; Pi et al., 2013; Grosso et al., 2015; Concina et al., 2019), but evidence that the modulation comes directly from the amygdala is sparse. We found that the BA-AC pathway is a likely conduit for information about valence to reach AC. This may have important short-term and long-term consequences for how the AC responds to behaviorally-significant sounds. Cohen et al. (2011) reported a significant influence of pup odor on responses to a variety of sounds. However, the design of their experiments precluded a trial-by-trial assessment of this influence. Instead, they recorded responses in alternating blocks lasting tens of minutes either with or without pup odor. We used an optogenetic approach that enabled precise optical control of BA inputs on the temporal scale of individual sounds. These experiments demonstrate that the BA projection is capable of rapidly modulating auditory responses. On the other hand, both odor presentation and optogenetic activation exhibited long-term experience dependence in several respects. Modulation of the AC by pup odor was only observed in mice with pup experience, not naïve virgin mice. In our experiments, pup odor responses in the BA (at least in head-fixed surrogates) were only evident prior to pup exposure. Moreover, after pup exposure, the effects of activating BA inputs shifted from being predominantly inhibitory to predominantly excitatory. This strongly implies that the

intrinsic circuitry of the AC and/or how it is accessed by BA afferents undergo long-term plasticity (Chavez et al., 2013; Yang et al., 2016). It also raises the possibility that pup odor may indeed be an important trigger for AC plasticity that has been commonly observed following maternal experience.

Behavioral function of basal amygdala

The BA is activated during maternal behavior and in response to multimodal pup stimuli. Presenting mothers with either a hypothermic pup or the combination of pup odors and USVs results in significantly elevated *c-fos* expression in the BA relative to controls presented with no stimulus (Okabe et al., 2013). In that study, the synaptic targets of pup-responsive BA neurons were not identified, but the BA has been suggested to influence appetitive maternal behaviors (e.g. retrieval) through its projections to nucleus accumbens and ventral pallidum (Numan and Stolzenberg, 2009; Numan and Young, 2016). Our results here argue that, in addition to regulating reward circuitry, the BA might contribute to goal-directed maternal behaviors in a previously unappreciated manner by regulating auditory processing of USVs.

Aside from its specific relationship to maternal behavior, recent evidence more broadly implicates the BA in regulating affiliative processes such as sociability and responses to social novelty (Mesquita et al., 2016; Huang et al., 2020). The BLA generally computes positive and negative valence signals (O'Neill et al., 2018) and emotional salience (Sengupta et al., 2018), and it is critical for motivated behavior. Distinct subsets of BLA neurons respond to either aversive or appetitive conditioned and unconditioned stimuli (Paton et al., 2006; Belova et al., 2007; Belova et al., 2008; Beyeler et al., 2018). Each subset tends to preferentially access different downstream targets (Senn et al., 2014; Namburi et al., 2015). Many BLA neurons exhibit positive (or negative)

responses to multiple positive (or negative) stimuli, suggesting that they encode valence independent of the specific stimulus (Gore et al., 2015). Less is known about activity in the BMA, but it may be more closely linked to controlling behavioral aversion (Adhikari et al., 2015; Ineichen et al., 2020). Finally, analysis of ensembles embedded in a large population of simultaneously recorded BA neurons across diverse behavioral conditions show that these ensembles adopt distinct network configurations to encode long-term behavioral states such as social or spatial exploration (Grundemann et al., 2019; Fustinana et al., 2021).

It is not known what computed quantities are represented by BA neurons that project to the AC, but all of the above observations reveal characteristics that they may share with other BA neurons. In any case, BA-AC neurons seem unlikely to carry straightforward sensory responses to odors. Given the known properties of the BA, they likely represent more abstract affective or state variables. We propose that the direct modulation of primary sensory activity with respect to these variables constitutes an underappreciated function of the amygdala.

Future work

This work raises several interesting questions for future study. First, how are the population signals we detect here distributed among individual BA-AC neurons? Do they share the reported properties of other BA neurons? Recording from or imaging many identified individual neurons simultaneously during maternal behavior could help answer those questions. Second, are there state changes during maternal behavior such as arousal or engagement that could be in part modulated by the BA, affecting the responses to vocal signals. Future experiments might therefore focus on large-scale network dynamics in AC during maternal interactions and how they are altered by inputs from BA. Third, are the odor signals from the BA that are shared with the AC also sent

to other targets of BA, including reward circuits in the ventral pallidum and nucleus accumbens, and what effect do they have there?

MATERIALS AND METHODS

Animals. All procedures were conducted in accordance with the National Institutes of Health's Guide for the Care and Use of Laboratory Animals and approved by the Cold Spring Harbor Laboratory Institutional Animal Care and Use Committee. All experiments were performed on adult (aged 6-12 weeks) female mice that were maintained on a 12h:12h light-dark cycle and received food *ad libitum*. Most mice were CBA/CaJ (Jax #000654), however some neuroanatomical tracing experiments were performed in H2B-GFP *(Rosa26-stop^{flox}-H2B-GFP,* gift from Bo Li), VGlut1Cre (*Slc17a7$^{tm1.1(cre)Hze}$/J*; Jax #023527), VGlut2Cre (*Slc17a6$^{tm2(cre)Lowl}$/J*; Jax #016963), or VGatCre (*Slc32a1$^{tm2(cre)Lowl}$/J*; Jax #016962). We performed all behavioral experiments during the dark cycle.

Retrieval behavior. Surrogates were generated by co-housing a virgin female with a pregnant CBA/CaJ dam beginning 1-5 days prior to birth. Pup retrieval behavior performance was first assayed on the day pups were born (P0) and again on P3 and P5 as described (Krishnan et al., 2017). Briefly, behavior was performed in the home cage (39 cm by 20 cm by 16 cm), which was placed in a larger dark, sound attenuated chamber (61 cm by 58 cm by 56 cm). The mother was removed and a surrogate was allowed to habituate to the behavior chamber in its home cage for 5 min with 5 pups in the nest. Pups were then removed for 2 minutes, and subsequently returned to all four corners and the center. The trial started when the last pup was placed and each surrogate was given 5 minutes to retrieve all pups back to the nest. Videos were recorded in the dark under infrared light using a Logitech webcam (c920) with the IR filter removed.

Behavioral videos were annotated using BORIS (Behavior Observation Research Interactive Software) (Friard et al., 2016) by a trained observer who was blind to the experimental condition and day of testing. The observer manually scored the onset and offset of events including

'search', 'retrieval success', 'retrieval error', 'investigation', 'air sniff', and 'nesting', which were exported to MATLAB for further analysis. A normalized latency score was calculated using the following formula:

$$norm.latency = \frac{\sum(t_1 - t_0), (t_2 - t_0), \ldots, (t_n - t_0)}{n \times L}$$

n = number of pups outside the nest, t_0 = start of the trial, t_n = time the nth pup was gathered, L = trial length (300s).

MOE ablation. Following five days of maternal experience, surrogates were given an intraperitoneal (IP) injection of methimazole (MMZ; 50 mg/kg) (Millipore Sigma, #46429) dissolved in saline. We waited 7 days to allow sufficient time for the MOE to degenerate before retesting mice in the retrieval assay.

Surgical procedures. Before all surgical procedures, mice were initially anesthetized with an IP injection (1.25 ml/kg) of an 80:20 mixture of ketamine (100 mg/ml) and xylazine (20 mg/ml) and were stabilized in a stereotaxic frame. Anesthesia was maintained throughout by vaporized isoflurane (1 – 2% as needed).

Depending on the specific experiment, we injected one or more adeno-associated viruses (AAVs) into the auditory cortex and/or the basal amygdala, as described in Results. See Table 1 for specific constructs used, titers, serotype, ordering information, and injected volumes. See Table 2 for injection coordinates. After the target volume of virus was expelled, the injection pipette was slowly retracted from the brain. In mice prepared for fiber photometry, a 5 mm length of 200 μm optical fiber (0.39 NA, Thorlabs) was implanted 200 μm above the BA injection site before being secured with Metabond dental cement along with a titanium head fixation bar. The scalp was sutured shut and the mouse was given a dose of meloxicam (2 mg/mL) for analgesia.

Table 1

Viral construct	*Ordering info*	*Volume and titre*
AAVrg.CAG.tdTomato	Addgene cat#: 59462-AAVrg	0.45nL/injection site (6 total) of 1.3 x 10^{13} GC mL^{-1}
AAVrg.pmSyn1.EBFP.Cre	Addgene cat#: 5107-AAVrg	0.45nL of 5 x 10^{12} GC mL^{-1}
AAVrg.hSyn.Cre.WPRE.hGH	Addgene cat#: 105553-AAVrg	0.45nL of 1.2 x 10^{13} GC mL^{-1}
AAVrg.FLEX.tdTomato	Addgene cat#: 28306-AAVrg	0.45 nL of 7.5 x 10^{12} GC mL^{-1}
AAV5.syn.FLEX.GCaMP6s.WPRE	Addgene cat#: 100845-AAV5	200nL of 2.9 x 10^{13} GC mL^{-1}
AAV9.synP.DIO.EGFP.WPRE.hGH	Addgene cat#: 100043-AAV9	200nL of 4.3 x 10^{13} GC mL^{-1}
AAV9.CAGGS.Flex.ChR2.tdTomato.WPRE.SV40	UPenn	200nL

Table 2

Brain Region	*Coordinates* (measured from bregma unless noted)
Auditory Cortex	AP: -1.7, -2.1, -2.4mm ML: 4.0mm DV: -0.35, -0.55mm (from cortical surface)*
Basal Amygdala	AP: -1.5mm ML: 3.0mm DV: -5.4mm

Fiber photometry. Experiments were performed with a custom-built two-color fiber photometry system. The output from two LEDs (470nm/565nm; Doric) was focused into a fiber launch holding a 200 μm optical fiber (0.37 NA; Doric) that could be coupled to the implanted optical fiber via a lightweight, flexible cable during daily recording sessions. The LEDs were sinusoidally modulated 180 degrees out of phase at 211Hz and emitted green and red light was collected from the optical fiber. Each color was separated and bandpass filtered and was detected by a dedicated photoreceiver (#2151, Newport Corporation). Light delivered to the brain was measured at ~30 mW at the fiber tip.

Animals used in head-fixed recording sessions were habituated to fixation for 30-60 minutes once a day for 3-5 days prior to testing. At the start of each session, animals were connected to the patch cord and baseline signal was recorded for 2 minutes. Recordings from freely behaving mice were conducted identically with the exception that the cable attached to the head led to an optical swivel (Doric) to allow free movement. The signal from each photoreceiver was digitized at a sampling rate of 6100 Hz and acquired to a computer via a National Instruments DAQ device (NI-USB6211).

The raw data were used to calculate ΔF/F signals offline with custom written MATLAB code. First, the value at each peak in the sinusoidal signals was detected, resulting in an effective sampling rate of 211 Hz. Each signal was low pass filtered at 15Hz and fit to a double exponential decay function, which was subtracted to correct for photobleaching during the trial. To correct for any movement artifact, we used a robust regression to compute a linear function for predicting the activity-independent component of the green signal based on the red. This component, which was in most cases small, was subtracted from the green signal. Finally, the result was mean subtracted and then divided by the mean to calculate ΔF/F. ΔF/F signals were Z-scored across all recording sessions from each mouse to compare calcium activity from multiple animals and days. The notation 'z-dFF' is used here to distinguish Z-score normalized ΔF/F signals from raw ΔF/F signals ('dFF').

Odor Presentation. Controlled presentation of odors to awake, head-fixed mice was achieved with a custom-built olfactometer as described (Cazakoff et al., 2014). Briefly, mice were head-fixed to a frame with their nose positioned in front of an odor port on a 10 cm diameter foam wheel. The wheel permitted the animal to freely walk or run or remain still. To deliver monomolecular odors, clean oxygen flow was briefly redirected by a solenoid assembly through the headspace of one of eight vials containing one odor (Table 5) diluted to 5% V/V in mineral oil. The odorized oxygen was mixed (1:10) with a clean air carrier stream to achieve a flow dilution of 0.5% saturated vapor. Pup and nesting material odors were presented by placing 3 pups or clean nesting material in a sealed chamber (4 oz mason jar) and swapping it with one of the odor vials in our olfactometer. Half of the pup chamber was kept on a warm pad and pup odor trials were limited to 10 minutes per session for the pups' safety and comfort. Pups used for odor stimulation

were used a maximum of 6 sessions per day and were returned to their mothers immediately following the experiment.

Table 3 Odorant Stimuli

Odorant	**Sigma catalog #**
Mineral Oil	330779
Amyl Acetate	W504009
Ethyl Tiglate	W246000
R-Carvone	124931
S-Carvone	435759
Pup	N/A
Clean Bedding	Bed r'Nest

USV recording and playback. Single pup vocalizations and tones were presented during electrophysiology recordings using one of the output channels of a National Instruments DAQ (NI-USB 6211) controlled by custom software written in MATLAB. Output was sent to an electrostatic speaker driver powering an electrostatic speaker (ED1/ES1, Tucker-Davis Technologies) positioned 4 inches behind the animal's head. Stimuli were low pass filtered and amplified at 100kHz using a custom filter and preamp (Kiwa Electronics). A sound level meter (Model 407736, 'A' weighting; Ex-Tech) was used to calibrate the RMS for all stimuli to 70 dB SPL at the head. USVs were detected using a polarized condenser ultrasound microphone (CM16/CMPA, Avisoft Bioacoustics) placed 12" above the cage floor and were digitally sampled at 200 kHz via a National Instruments DAQ (NI-USB 6211) using custom software written in MATLAB.

Electrophysiology. Prior to recording, the mouse was anesthetized with an 80:20 mixture (1.25ml/kg) of ketamine (100mg/ml) and xylazine (20 mg/ml). Extracellular recordings were made using the 'loose patch' method (Cazakoff et al., 2014; Lau et al., 2020). Micropipettes were pulled from borosilicate glass filaments (O.D. 1.5mm, I.D. 0.86mm; BF150-86-10, Sutter Instrument) using a Flaming/Brown micropipette puller (P-97; Sutter Instruments) and back-filled with intracellular solution (125 mM potassium gluconate, 10mM potassium chloride, 2mM magnesium chloride, and 10mM HEPES pH 7.2) for a final resistance of 10 – 30 MΩ. Isolated single unit neural activity was recorded using a BA-03X bridge amplifier (npi), low-pass filtered at 3 kHz, digitized at 10 kHz, and acquired using Spike2 software (v.7; Cambridge Electronic Design). Recording depth was measured by a piezoelectric micromanipulator (Sutter Instrument SOLO/E-116). All neurons were found from 300 μm – 1200 μm from the cortical surface, corresponding to approximately layers II – VI of auditory cortex.

Experiments were performed in an anechoic, sound attenuated chamber (Industrial Acoustics). Single pup vocalizations and tones were presented to surrogates using one of the output channels on a Power1401 ADC/DAC board (Cambridge Electronic Design). Stimuli were low pass filtered at 100kHz and amplified using a custom filter and preamp (Kiwa Electronics). Output was sent to an electrostatic speaker driver powering an electrostatic speaker (ED1/ES1, Tucker-Davis Technologies) positioned 4 inches in front of the animal. All stimuli were calibrated to RMS of 65dB SPL at the animal's head using a sound level meter (Ex-Tech, model 407736). Stimuli consisted of 7 log-spaced pure tones (16, 20, 25, 32, 40, 50, 64 kHz) or 8 natural pup calls recorded from CBA/CaJ mouse pups on postnatal day 2 (calls 1-4) or 4 (calls 5-8). Stimuli were presented for 100ms at an interstimulus interval of 4s.

Optogenetic stimulation. To optogenetically activate BA terminals in the auditory cortex, the tip of an optical fiber (Ø 400 µm NA 0.39; Thor Labs) was positioned just over the craniotomy with a micromanipulator such that light shone directly on the cortical surface. Trains of light pulses were controlled by the timing output of an isolated pulse stimulator (A-M Systems) and consisted of 10 ms pulses of blue light (473nm; OEM laser) delivered at 20 Hz for 1 s (Kim et al., 2016; Millan et al., 2017) and beginning 500 ms prior to the auditory stimulus. Laser power was 30 mW as measured at the tip of the optic fiber. Based on this, we estimate the power to be 2 – 10 mW/mm^2 at a depth of 300-1000 mm from the cortical surface (Yizhar et al., 2011), where most recordings were made.

Post-mortem histology and immunohistochemistry. At the end of each experiment, mice were delivered a lethal dose of pentobarbital (Euthasol), and then exsanguinated and transcardially perfused with PBS followed by 4% paraformaldehyde. In cases where the tissue was required for staining and/or microscopy, the brain and the main olfactory epithelium (MOE) were extracted and post-fixed overnight at 4°C. Brains were then transferred to a solution of 30% sucrose in PBS overnight at room temperature (RT) and subsequently sectioned on a freezing microtome at a thickness of 50µm. For visualization of GCaMP6s expression, brain sections were first incubated with a primary antibody raised against GFP in chicken (AVES) diluted 1:1000 in PDT (0.5% normal donkey serum, 0.1% Triton X-100 in PBS) at 4 degrees overnight and then stained with a secondary anti-chicken Alexa 488 fluorophore raised in goat and diluted 1:500 in PDT for 2 h at room temperature. Nasal tissue was dissected from the skull (Dunston et al., 2013) and sent to the CSHL histology core to be paraffin sectioned, H&E stained, and compared to a saline injected control (Figure 1). MOE ablation was confirmed by manual inspection of the processed tissue.

Data analysis. All data analysis was performed with either Matlab (Mathworks) or Prism 9 software (GraphPad). Unless otherwise noted, data are reported as mean ± standard error. Electrophysiology data were manually spike sorted into single unit spike trains with Spike2 (CED). All subsequent analyses were performed with custom-written code in MATLAB (Mathworks). Mean baseline firing rate was calculated as the mean spontaneous firing rate during a 1 s period just before each stimulus. This quantity was subtracted from the stimulus-evoked spike rate measured from 50 – 200 ms after the onset of each stimulus to calculate 'response strength.' Neurons that were presented fewer than 6 trials or had a mean firing rate of less than 0.5 spikes per trial were excluded from analysis, unless they exhibited clear auditory responses. To assess the statistical significance of responses to each auditory stimulus, we used a bootstrap procedure. For a response window length t, and a stimulus presented n times, we created a null distribution by computing the mean response strength across n windows of length t, randomly drawn from the full spike record and repeating this 10,000 times. Auditory-evoked response strengths in the top or bottom 2.5% of the null distribution were considered significantly excitatory or inhibitory auditory-evoked responses, respectively.

ROC analysis was used to assess whether the distribution of auditory-evoked response sttrengths from light-on trials were discriminable from light-off trials for a given neuron and stimulus. Analysis was performed in MATLAB (Mathworks) using a publicly available ROC curve function (Marínez-Cagigal, 2018). Because optogenetic modulation of auditory-evoked responses could be either enhancing or suppressive, we converted all auROC values < 0.5 to 1 minus their value.

To determine the degree to which optogenetic stimulation modified the firing response for each cell-stimulus pair that exhibited an auditory response, we used the following formula to

calculate a modulation index. Here, RS_{aud} equals the mean response strength to a given stimulus without optogenetic stimulation, and $RS_{opto.}$ equals the mean response strength in response to the same stimulus with optogenetic stimulation.

$$MI = \frac{RS_{aud} - RS_{opto}}{RS_{aud} + RS_{opto}}$$

Optogenetic modulation of auditory responses was categorized as either enhancing or suppressive. This classification was based on whether the mean auditory-evoked response strength during optogenetic stimulation was higher or lower than the response strength evoked by the auditory stimulus alone.

For the analysis of odor-evoked activity, we calculated the mean amplitude of the z-dFF signal over the 4 s following the onset of odor presentation, and compared that to 2 s of baseline that occurred immediately before odor onset. We also calculated the difference between the mean signal at these two time points.

To examine whether an individual cell exhibited an evoked response to light stimulation alone (without auditory stimulus), we combined data from all light-only trials collected from a single cell. We then calculated the mean response strength within the 1s window of light stimulation and assessed whether the cell exhibited a statistically significant response based on the bootstrap procedure described earlier.

REFERENCES

Adhikari A, Lerner TN, Finkelstein J, Pak S, Jennings JH, Davidson TJ, Ferenczi E, Gunaydin LA, Mirzabekov JJ, Ye L, Kim SY, Lei A, Deisseroth K (2015) Basomedial amygdala mediates top-down control of anxiety and fear. Nature 527:179-185.

Belova MA, Paton JJ, Salzman CD (2008) Moment-to-moment tracking of state value in the amygdala. J Neurosci 28:10023-10030.

Belova MA, Paton JJ, Morrison SE, Salzman CD (2007) Expectation modulates neural responses to pleasant and aversive stimuli in primate amygdala. Neuron 55:970-984.

Beyeler A, Chang CJ, Silvestre M, Leveque C, Namburi P, Wildes CP, Tye KM (2018) Organization of Valence-Encoding and Projection-Defined Neurons in the Basolateral Amygdala. Cell Rep 22:905-918.

Canteras NS, Simerly RB, Swanson LW (1995) Organization of projections from the medial nucleus of the amygdala: a PHAL study in the rat. J Comp Neurol 360:213-245.

Carcea I et al. (2021) Oxytocin neurons enable social transmission of maternal behaviour. Nature 596:553-557.

Cazakoff BN, Lau BY, Crump KL, Demmer HS, Shea SD (2014) Broadly tuned and respiration-independent inhibition in the olfactory bulb of awake mice. Nat Neurosci 17:569-576.

Chavez CM, McGaugh JL, Weinberger NM (2009) The basolateral amygdala modulates specific sensory memory representations in the cerebral cortex. Neurobiol Learn Mem 91:382-392.

Chavez CM, McGaugh JL, Weinberger NM (2013) Activation of the basolateral amygdala induces long-term enhancement of specific memory representations in the cerebral cortex. Neurobiol Learn Mem 101:8-18.

Cohen L, Mizrahi A (2015) Plasticity during motherhood: changes in excitatory and inhibitory layer 2/3 neurons in auditory cortex. J Neurosci 35:1806-1815.

Cohen L, Rothschild G, Mizrahi A (2011) Multisensory integration of natural odors and sounds in the auditory cortex. Neuron 72:357-369.

Concina G, Renna A, Grosso A, Sacchetti B (2019) The auditory cortex and the emotional valence of sounds. Neurosci Biobehav Rev 98:256-264.

David SV, Fritz JB, Shamma SA (2012) Task reward structure shapes rapid receptive field plasticity in auditory cortex. Proc Natl Acad Sci U S A 109:2144-2149.

Dunston D, Ashby S, Krosnowski K, Ogura T, Lin W (2013) An effective manual deboning method to prepare intact mouse nasal tissue with preserved anatomical organization. J Vis Exp.

Ehret G, Haack B (1981) Categorical perception of mouse pup ultrasound by lactating females. Naturwissenschaften 68:208-209.

Ehret G, Koch M, Haack B, Markl H (1987) Sex and parental experience determine the onset of an instinctive behavior in mice. Naturwissenschaften 74:47.

Fraser EJ, Shah NM (2014) Complex chemosensory control of female reproductive behaviors. PLoS One 9:e90368.

Friard O, Gamba M, Fitzjohn R (2016) BORIS: a free, versatile open-source event-logging software for video/audio coding and live observations. Methods in Ecology and Evolution 7:1325-1330.

Fustinana MS, Eichlisberger T, Bouwmeester T, Bitterman Y, Luthi A (2021) State-dependent encoding of exploratory behaviour in the amygdala. Nature 592:267-271.

Galindo-Leon EE, Lin FG, Liu RC (2009) Inhibitory plasticity in a lateral band improves cortical detection of natural vocalizations. Neuron 62:705-716.

Gore F, Schwartz EC, Brangers BC, Aladi S, Stujenske JM, Likhtik E, Russo MJ, Gordon JA, Salzman CD, Axel R (2015) Neural Representations of Unconditioned Stimuli in Basolateral Amygdala Mediate Innate and Learned Responses. Cell 162:134-145.

Grosso A, Cambiaghi M, Renna A, Milano L, Roberto Merlo G, Sacco T, Sacchetti B (2015) The higher order auditory cortex is involved in the assignment of affective value to sensory stimuli. Nat Commun 6:8886.

Grundemann J, Bitterman Y, Lu T, Krabbe S, Grewe BF, Schnitzer MJ, Luthi A (2019) Amygdala ensembles encode behavioral states. Science 364.

Hernandez-Miranda LR, Ruffault PL, Bouvier JC, Murray AJ, Morin-Surun MP, Zampieri N, Cholewa-Waclaw JB, Ey E, Brunet JF, Champagnat J, Fortin G, Birchmeier C (2017) Genetic identification of a hindbrain nucleus essential for innate vocalization. Proc Natl Acad Sci U S A 114:8095-8100.

Huang WC, Zucca A, Levy J, Page DT (2020) Social Behavior Is Modulated by Valence-Encoding mPFC-Amygdala Sub-circuitry. Cell Rep 32:107899.

Ineichen C, Greter A, Baer M, Sigrist H, Sautter E, Sych Y, Helmchen F, Pryce CR (2020) Basomedial amygdala activity in mice reflects specific and general aversion uncontrollability. Eur J Neurosci.

Kim J, Pignatelli M, Xu S, Itohara S, Tonegawa S (2016) Antagonistic negative and positive neurons of the basolateral amygdala. 19.

Krishnan K, Lau BY, Ewall G, Huang ZJ, Shea SD (2017) MECP2 regulates cortical plasticity underlying a learned behaviour in adult female mice. Nat Commun 8:14077.

Lau BYB, Krishnan K, Huang ZJ, Shea SD (2020) Maternal experience-dependent cortical plasticity in mice is circuit- and stimulus-specific and requires MECP2. J Neurosci.

Marínez-Cagigal V (2018) ROC Curve. In, 3.1 Edition. MATLAB Central File Exchange.

Mesquita LT, Abreu AR, de Abreu AR, de Souza AA, de Noronha SR, Silva FC, Campos GS, Chianca DA, Jr., de Menezes RC (2016) New insights on amygdala: Basomedial amygdala regulates the physiological response to social novelty. Neuroscience 330:181-190.

Millan EZ, Kim HA, Janak PH (2017) Optogenetic activation of amygdala projections to nucleus accumbens can arrest conditioned and unconditioned alcohol consummatory behavior. Neuroscience 360:106-117.

Miranda JA, Liu RC (2009) Dissecting natural sensory plasticity: hormones and experience in a maternal context. Hear Res 252:21-28.

Namburi P, Beyeler A, Yorozu S, Calhoon GG, Halbert SA, Wichmann R, Holden SS, Mertens KL, Anahtar M, Felix-Ortiz AC, Wickersham IR, Gray JM, Tye KM (2015) A circuit mechanism for differentiating positive and negative associations. Nature 520:675-678.

Numan M, Stolzenberg DS (2009) Medial preoptic area interactions with dopamine neural systems in the control of the onset and maintenance of maternal behavior in rats. Front Neuroendocrinol 30:46-64.

Numan M, Young LJ (2016) Neural mechanisms of mother-infant bonding and pair bonding: Similarities, differences, and broader implications. Horm Behav 77:98-112.

Numan M, Bress JA, Ranker LR, Gary AJ, Denicola AL, Bettis JK, Knapp SE (2010) The importance of the basolateral/basomedial amygdala for goal-directed maternal responses in postpartum rats. Behav Brain Res 214:368-376.

O'Neill PK, Gore F, Salzman CD (2018) Basolateral amygdala circuitry in positive and negative valence. Curr Opin Neurobiol 49:175-183.

Okabe S, Nagasawa M, Kihara T, Kato M, Harada T, Koshida N, Mogi K, Kikusui T (2013) Pup odor and ultrasonic vocalizations synergistically stimulate maternal attention in mice. Behav Neurosci 127:432-438.

Paton JJ, Belova MA, Morrison SE, Salzman CD (2006) The primate amygdala represents the positive and negative value of visual stimuli during learning. Nature 439:865-870.

Perry CJ, McNally GP (2013) A role for the ventral pallidum in context-induced and primed reinstatement of alcohol seeking. Eur J Neurosci 38:2762-2773.

Petrovich GD, Risold PY, Swanson LW (1996) Organization of projections from the basomedial nucleus of the amygdala: a PHAL study in the rat. J Comp Neurol 374:387-420.

Pi HJ, Hangya B, Kvitsiani D, Sanders JI, Huang ZJ, Kepecs A (2013) Cortical interneurons that specialize in disinhibitory control. Nature 503:521-524.

Rosenblatt JS (1967) Nonhormonal basis of maternal behavior in the rat. Science 156:1512-1514.

Sengupta A, Yau JOY, Jean-Richard-Dit-Bressel P, Liu Y, Millan EZ, Power JM, McNally GP (2018) Basolateral Amygdala Neurons Maintain Aversive Emotional Salience. J Neurosci 38:3001-3012.

Senn V, Wolff SB, Herry C, Grenier F, Ehrlich I, Grundemann J, Fadok JP, Muller C, Letzkus JJ, Luthi A (2014) Long-range connectivity defines behavioral specificity of amygdala neurons. Neuron 81:428-437.

Stolzenberg DS, Champagne FA (2016) Hormonal and non-hormonal bases of maternal behavior: The role of experience and epigenetic mechanisms. Horm Behav 77:204-210.

Wang Z, Storm DR (2011) Maternal behavior is impaired in female mice lacking type 3 adenylyl cyclase. Neuropsychopharmacology 36:772-781.

Weiss J, Pyrski M, Jacobi E, Bufe B, Willnecker V, Schick B, Zizzari P, Gossage SJ, Greer CA, Leinders-Zufall T, Woods CG, Wood JN, Zufall F (2011) Loss-of-function mutations in sodium channel Nav1.7 cause anosmia. Nature 472:186-190.

Yang Y, Liu DQ, Huang W, Deng J, Sun Y, Zuo Y, Poo MM (2016) Selective synaptic remodeling of amygdalocortical connections associated with fear memory. Nat Neurosci 19:1348-1355.

Yizhar O, Fenno LE, Prigge M, Schneider F, Davidson TJ, O'Shea DJ, Sohal VS, Goshen I, Finkelstein J, Paz JT, Stehfest K, Fudim R, Ramakrishnan C, Huguenard JR, Hegemann P, Deisseroth K (2011) Neocortical excitation/inhibition balance in information processing and social dysfunction. Nature 477:171-178.

FIGURE LEGENDS

Figure 1: Olfactory signals from the main olfactory system are essential to maintain pup retrieval in surrogates. (a) Experimental timeline. (b) Schematic of retrieval assay. (c) Plot of latency index over time. Nulliparous female mice (n = 5) were assessed for pup retrieval as described prior to any exposure to pups ('naïve'), on days P0, P3 and P5 relative to the birth of the pups with which they were co-housed, and again 7 days after a single IP injection of MMZ (50 mg/kg). Latency index scores (mean ± SEM) were naïve: 0.622 ± 0.0, P0: 0.413 ± 0.163, P3: 0.060 ± 0.01, P5: 0.052 ± 0.01, and MMZ: 0.872 ± 0.08. All pairwise comparisons were performed using Tukey's multiple comparisons test (* $p < 0.05$, ** $p < 0.01$). Any comparisons not depicted were not

significant ($p > 0.05$). (d) Bar plot comparing the percentage of pups retrieved among naïve mice, surrogates on P5, and surrogates after MMZ treatment. Pairwise comparisons were performed using Tukey's multiple comparisons test (** $p < 0.01$) (e) Plot of latency index comparing pre-MMZ performance when retrieving the familiar, co-housed pups and a novel set of pups. A pairwise comparison of these values showed no significant difference (Wilcoxon matched-pairs signed rank test, $p = 0.625$). (f) Photomicrographs comparing representative paraffin-embedded, H&E stained sections of the main olfactory epithelium from a mouse that received an injection of MMZ and a mouse that received a control injection of saline (scale bar = 200 μm).

Figure 2: A subpopulation of glutamatergic neurons in the BA project to the AC. (a) Retrograde tracing of AAVrg-CAG-tdTomato from the AC reveals cell bodies labeled within the BA, (b) throughout the ipsilateral AC, (c) contralateral AC, and (d) medial geniculate body (scale bars = 500 μm). (e) Unrestricted retrograde tracing of AAVrg-hSyn-Cre-WPRE.hGH from the AC of a H2B-GFP mouse yields GFP positive nuclear staining for quantification of BA neurons that project to the AC (scale bars = 500 μm). (f) Cre-restricted tracing of AAVrg-FLEX-tdTomato from the AC in vGlut1Cre mouse line (scale bars = 500 μm). (g) Quantification of tracer positive neurons as a result of retrograde tracing from the AC in unrestricted (H2B-GFP, 4513 ± 1977 neurons) and Cre-restricted mouse lines (vGlut1 256.3 ± 43.17 neurons; vGlut2 380.3 ± 23.99 neurons; vGAT 0 ± 0 neurons) revealed significantly fewer tracer positive neurons in vGlut2 animals compared to H2B-GFP (Mann-Whitney test, $p = 0.0238$).

Figure 3: Auditory cortex-projecting BA neurons respond to odors including the odor of pups. (a) Intersectional viral strategy. The retrograde virus AAVrg-hSyn-Cre-WPRE-hGH was injected into

the AC and at the same time, the Cre-dependent AAV5-syn-FLEX-GCaMP6s-WPRE was injected into the BA. This ensured that GCaMP was only expressed in BA neurons that project to the AC. We also implanted an optical fiber into BA during the same surgery. (b) Experimental setup for measuring odor responses. Mice were fixed to a frame by a titanium bar cemented to their skull, and they were allowed to freely run or remain still on a foam wheel. Chemical odors were presented by directing airflow from the head space of a glass vial to the mouse's nose. On other trials, the same was done with a small jar containing pups and/or bedding. (c) Example traces of dFF in response to multiple 2 s odor presentations from the same mouse before and after MMZ treatment. The colored bars above each trace denote the time of an odor trial. Black bars denote a blank (mineral oil) trial. (d) Heat plot of mean responses to all odors by all mice. Each row in the plot represents the mean response over multiple trials to one odor in one mouse (odor-mouse pair), expressed as a Z score (z-dFF), according to the color bar. Rows are ordered by the magnitude of each response. (e) Plot of mean response across all mice for each of four monomolecular odors that were presented. Odors are as follows: AA – amyl acetate, ET – ethyl tiglate, RC – R-carvone, SC – S-carvone. Each point denotes the mean response of one mouse, defined as the difference from pre-stimulus baseline (2 s). The distributions of responses for all odors were significantly different from 0 (n = 8 mice, Wilcoxon signed rank test, ** $p < 0.01$). (f) Plot of mean response across all mice for each of four monomolecular odors that were presented after ablation of the MOE with MMZ treatment. Each point denotes the mean response of one mouse, defined as the difference from pre-stimulus baseline. None of the distributions of responses for any odors significantly differed from 0 (n = 5 mice, Wilcoxon signed rank test, $p \geq 0.05$). (g) Heatplot of mean responses to pup odor for each mouse. Each row in the lower plot represents the mean response over multiple trials to pup odor in one mouse, expressed as a Z score (z-dFF), according

to the color bar. Rows are ordered by the magnitude of each response. The upper plot shows a trace of the mean ± SEM response to pups across all mice (gray) and the mean ± SEM response to pups in the same mice following ablation of the MOE with MMZ injection. (h) Plot of mean response across all mice for pup odor, comparing responses in naïve females, at the end of 5 d surrogacy, and after ablation of the MOE with MMZ treatment. Each point denotes the mean response of one mouse, defined as the difference from pre-stimulus baseline. The distribution of responses to pup odor was significantly different from 0 in naïve mice (n = 6 mice; 0.634 ± 0.249 z-dFF, Wilcoxon signed rank test, $p = 0.0312$). Responses to pup odor did not significantly differ from 0 after surrogacy or MMZ treatment (surrogates: n = 6 mice; 0.080 ± 0.173 z-dFF, MMZ: n = 5 mice, 0.163 ± 0.091 z-dFF, Wilcoxon signed rank test, $p \geq 0.05$).

Figure 3 – Figure supplement 1: Fiber placement for fiber photometry subjects. (a) A series of atlas sections showing fiber placement for all fiber photometry subjects (n = 8). The red bars on the sections denote where the fiber tips were placed. (b) A representative photomicrograph showing the placement of one fiber relative to amygdala structures (BA: basal amygdala, LA: lateral amygdala, scale bar = 500 μm).

Figure 3 – Figure supplement 2: Olfactory responses are variable across odors and mice. (a) Plots of the responses of all mice separately to each of four monomolecular odorants. In each plot, the upper panel is a mean trace of the responses of all mice to one monomolecular odor (gray) and the response to the same odor in a subset of those mice following ablation of the MOE with MMZ injection (red). The shaded area around each trace marks the SEM of the response. (b) Heatplot of mean responses to nest material for each mouse. Each row in the lower plot represents the mean

response over multiple trials to nest material in one mouse, expressed as a Z score (z-dFF), according to the color bar. Rows are ordered by the magnitude of each response. The upper plot shows a trace of the mean ± SEM response to nest material across all mice (gray) and the mean ± SEM response to nest material in the same mice following ablation of the MOE with MMZ injection. (c) Plot of mean response across all mice for nest material, comparing responses in naïve females, at the end of 5 d surrogacy, and after ablation of the MOE with MMZ treatment. Each point denotes the mean response of one mouse, defined as the difference from pre-stimulus baseline. The distribution of responses to nest material was significantly different from 0 in naïve mice (n = 6 mice; 0.513 ± 0.181 z-dFF, Wilcoxon signed rank test, $p = 0.031$) and surrogates (n = 6 mice; 0.432 ± 0.051 z-dFF, Wilcoxon signed rank test, $p = 0.031$). Responses to nest material did not significantly differ from 0 after MMZ treatment (n = 5 mice; 0.210 ± 0.096 z-dFF, Wilcoxon signed rank test, $p = 0.125$).

Figure 3 – Figure supplement 3: Mice expressing activity-independent GFP in BA-AC show no detectable odor responses. (a) Plot of mean response across all mice for all odors, comparing baseline z-dFF to mean z-dFF during all odor presentations for mice that expressed GFP in BA-AC instead of GCaMP6s. Each pair of points indicates the mean fluorescence at baseline of one mouse and mean fluorescence during odor trials for the same mouse. These values were not significantly different (n = 5 mice; 0.044 ± 0.0167 z-dFF, paired t test, $p = 0.815$). (b) Plot of mean response across all GFP-expressing mice for four monomolecular odors (AA – amyl acetate, ET – ethyl tiglate, RC – R-carvone, SC – S-carvone), pup odor, and nest material. Each point denotes the mean response of one mouse, defined as the difference from pre-stimulus baseline (2 s). None

of the distributions of responses for any of the odors were significantly different from 0 (n = 5 mice, Wilcoxon signed rank test, $p \geq 0.05$).

Figure 4: BA-AC neurons show elevated activity during pup search that terminates with pup contact. (a) Example traces of dFF during several episodes of searching for pups. Each trace is taken from a different mouse on a different postnatal day (shown to the upper left of each trace). The colored bars above each trace denote time spent searching for a pup, beginning at the time the female exits the nest and ending at the time she contacts a pup. The blue bars are above traces taken from mice expressing GCaMP in BA-AC neurons. The trace with the green bars above it was taken from a mouse that was expressing GFP in BA-AC neurons. (b) Average data across all retrieval trials from one mouse aligned to the end of search. The upper panel is a heat map of z-dFF for 27 retrieval events taken from P0, P1, P3, and P5. Each row depicts one retrieval event aligned to the end of the search, when the mouse contacts the pup (vertical dashed line). Color is mapped to z-dFF according to the color bar on the lower right. The lower panel is a plot of mean z-dFF for all trials. The shaded area around the trace denotes the SEM of the response. Note the abrupt decrease in activity as the female encounters the pup. (c) Plot summarizing the average response to pup contact in all mice. The upper panel is a heatmap of the average response to a search that terminates in an encounter with a pup across all trials for all mice (n = 9). Each row is the mean response to pup contact (vertical dashed line) for one mouse, calculated as in (b). Color is mapped to z-dFF according to the color bar on the lower right. The lower panel is a plot of mean z-dFF for all mice. The shaded area around the trace denotes the SEM of the response. (d) Plot of the mean change in fluorescence associated with several events (search, pup contact, investigation, and air sniff) across all mice. Each point denotes the mean response of one mouse, defined as the

difference between the mean fluorescence during the first 3 s after each event and the mean value during the immediately preceding 3 s. Mean activity during search (0.1863 ± 0.076 z-dFF), after pup contact (-0.284 ± 0.068 z-dFF), and during investigation (-0.126 ± 0.040 z-dFF) were significantly different from 0 (n = 10 mice; Wilcoxon signed rank test, $*p < 0.05$, $**p < 0.01$). No significant change in fluorescence was detected when the mouse sniffed the air (n = 10 mice; -0.028 ± 0.057 z-dFF, Wilcoxon signed rank test, $p = 0.695$) or in mice that expressed activity-independent GFP in the BA (n = 4; 0.030 ± 0.092 z-dFF, Wilcoxon signed rank test, $p > 0.999$).

Figure 5: Optogenetic activation of the BA-AC pathway elicits widespread and bidirectional modulation of auditory responses in the auditory cortex. (a) Schematic of the experimental design. The same intersectional strategy for labeling BA-AC neurons with GCaMP6s (Figure 3A) was used to express ChR2 in the same neurons. The retrograde virus AAVrg-hSyn-Cre-WPRE-hGH was injected into the AC and at the same time, the Cre-dependent AAV9-CAGS-FLEX-ChR2-tdT-WPRE-SV40 was injected into the BA. ChR2 expression was detected in axons in the AC. Mice were acutely anesthetized for electrophysiology recordings and presented with auditory stimuli including synthesized pure tones and previously recorded pup calls. Stimuli were presented in a pseudorandom order and 50% of trials for each stimulus were accompanied by a train of 473 nm light pulses (20 Hz) directed at the cortical surface to activate BA-AC terminals. (b) Plots comparing responses of an auditory cortical neuron to logarithmically spaced pure tones when presented during light activation of BA-AC and when presented alone. Data are from a naïve female. Each stimulus is associated with a raster plot and peristimulus time histogram (bin size = 50 ms) from control trials (top row) and from light activation trials (bottom row with blue shading). The blue shading denotes the duration of the light train relative to the tone. Note that responses to

the 25 kHz tone are significantly weaker when BA-AC terminals were activated by light (n = 8 trials; comparison of trials with and without light, unpaired t test with Bonferroni correction, $**p < 0.01$). (c) Line plot of data from (b) comparing the mean baseline-subtracted firing rate evoked by each tone on control trials (black) and on light trials (blue) ($**p < 0.01$). Vertical lines denote SEM. (c) Plots comparing responses of a different auditory cortical neuron to 8 different pup call exemplars when presented during light activation of BA-AC and when presented alone. Data are from a surrogate female. Panels are organized as in (b). (d) Line plot of data from (c) comparing the mean baseline-subtracted firing rate evoked by each call on control trials (black) and on light trials (blue). Note that in this case, responses to call 3 are significantly stronger when BA-AC terminals were activated by light (n = 8 trials; comparison of trials with and without light, unpaired t test with Bonferroni correction, $**p < 0.01$). (f) Distribution of auROC values for each cell-stimulus pair from ChR2 injected animals (blue) and GFP controls (green) separated by pup experience (naïve, left panel; surrogate, right panel). The mean value of each distribution is marked by the vertical line of corresponding color. (g) Box plots of the data in (f) demonstrate that ChR2 expressing animals exhibit significantly greater discriminability between light-on and light-off trials for both naïve virgins (ChR2: n = 415 cell-stimulus pairs, 0.623 ± 0.005; GFP: n = 376 cell-stimulus pairs, 0.574 ± 0.003, Mann-Whitney U-test, $p < 0.0001$) and surrogates (ChR2: n = 616 cell-stimulus pairs, 0.610 ± 0.005; GFP: n = 469 cell-stimuls pairs, 0.576 ± 0.003, Mann-Whitney U-test $p = 0.0005$).

Figure 5 – Figure supplement 1: Optogenetic activation of the BA-AC pathway elicits widespread and bidirectional modulation of auditory responses in the auditory cortex of surrogates. (a) Plots comparing responses of an auditory cortical neuron to logarithmically spaced pure tones

when presented during light activation of BA-AC and when presented alone. Data are from a surrogate female. Each stimulus is associated with a raster plot and peristimulus time histogram (bin size = 50 ms) from control trials (top row) and from light activation trials (bottom row with blue shading). The blue shading denotes the duration of the light train relative to the tone Note that responses to the 25 kHz tone are significantly stronger when BA-AC terminals were activated by light (n = 15 trials; comparison of trials with and without light, unpaired t test with Bonferroni correction, $^{**}p < 0.01$). (b) Line plot of data from (a) comparing the mean baseline-subtracted firing rate evoked by each tone on control trials (black) and on light trials (blue). Vertical lines denote SEM. (d) Plots comparing responses of a different auditory cortical neuron to 8 different pup call exemplars when presented during light activation of BA-AC and when presented alone. Data are from a naïve female. Panels are organized as in (b). (e) Line plot of data from (d) comparing the mean baseline-subtracted firing rate evoked by each call on control trials (black) and on light trials (blue). Note that responses to call 4 are significantly weaker when BA-AC terminals were activated by light (n = 20 trials; comparison of trials with and without light, unpaired t test with Bonferroni correction, $^{***}p < 0.001$).

Figure 6: The effects of BA-AC activation on AC neurons are experience-dependent. (a) Scatterplot of response strength (RS) comparing control trials versus light activation trials for all cell-stimulus pairs in naïve mice expressing ChR2 in BA-AC neurons. Tone stimuli are plotted as open circles and call stimuli are plotted as filled circles. (b) Scatterplot of response strength (RS) comparing control trials versus light activation trials for all cell-stimulus pairs in surrogate mice expressing ChR2 in BA-AC neurons. Tone stimuli are plotted as open circles and call stimuli are plotted as filled circles. (c) Box plot of modulation index comparing modulation of tone responses

in naïves (black) and surrogates (red) expressing ChR2 in BA-AC (naïve: n = 226 cell-stimulus pairs, -0.185 ± 0.037; surrogates: n = 291 cell-stimulus pairs, 0.031 ± 0.034; Mann-Whitney U test, $p < 0.0001$) (left side). On the right side, the box plot compares modulation of USV call responses in naives (black) and surrogates (red) (naïve: n = 175 cell-stimulus pairs, -0.110 ± 0.042, surrogate: n = 274 cell-stimulus pairs, 0.055 ± 0.032; Mann-Whitney U test, $p = 0.0006$ Mann-Whitney U test). (d) Box plot of modulation index comparing modulation of tone responses in naïves (dark green) and surrogates (light green) expressing GFP in BA-AC (naïve: n = 213 cell-stimulus pairs, -0.027 ± 0.031; surrogates: n = 223 cell-stimulus pairs, -0.005 ± 0.038; Mann-Whitney U test, $p = 0.453$) (left side). On the right side, the boxplot compares modulation of USV call responses in naives (black) and surrogates (red) (naïve: n = 153 cell-stimulus pairs, -0.078 ± 0.040, surrogate: n = 206 cell-stimulus pairs, -0.020 ± 0.030; Mann-Whitney U test, $p = 0.204$). (e) Example responses to light only trials for naïve and surrogate mice. The top panel shows a peristimulus time histogram (bin size = 50 ms) of the mean firing rate of an AC neuron in a naive female during 20 trials of light stimulation accompanied by silence. The bottom panel shows a peristimulus time histogram (bin size = 50 ms) of the mean firing rate of an AC neuron in a surrogate female during 20 trials of light stimulation accompanied by silence. (f) Swarm plot comparing the mean response to light only trials for all neurons in ChR2-expressing mice. (naïve: n = 34, -0.091 ± 0.089; surrogates: n = 49, 0.237 ± 0.101, Mann-Whitney U, $p = 0.0248$).

Figure 6 – Figure supplement 1: Optogenetic modulation of auditory responses occurs independent of stimulus frequency. (a) The percentage of auditory responses enhanced by optogenetic activation is generally higher in surrogates compared to naïve animals. For the majority of stimulus frequencies this effect is not statistically significant when comparing the

observed responses in ChR2 expressing animals to expected responses of GFP controls (Fisher's exact test, $p > 0.05$), with the exception of naïve responses to 32kHz frequency tones (Fisher's exact test, $p = 0.020$). (b) The same is true for call exemplars with the exception of surrogate responses to call exemplar 8 (Fisher's exact test, $p = 0.0003$). (c) The average modulation index across units (n = 31-33) recorded from naïve mice (n = 7) is not significantly different across frequencies (2way ANOVA, stimulus source of variation, p = 0.0569). (b) The same is true of units (n = 36-44) recorded from surrogates (n = 10, 2way ANOVA, stimulus source of variation, p = 0.6677).

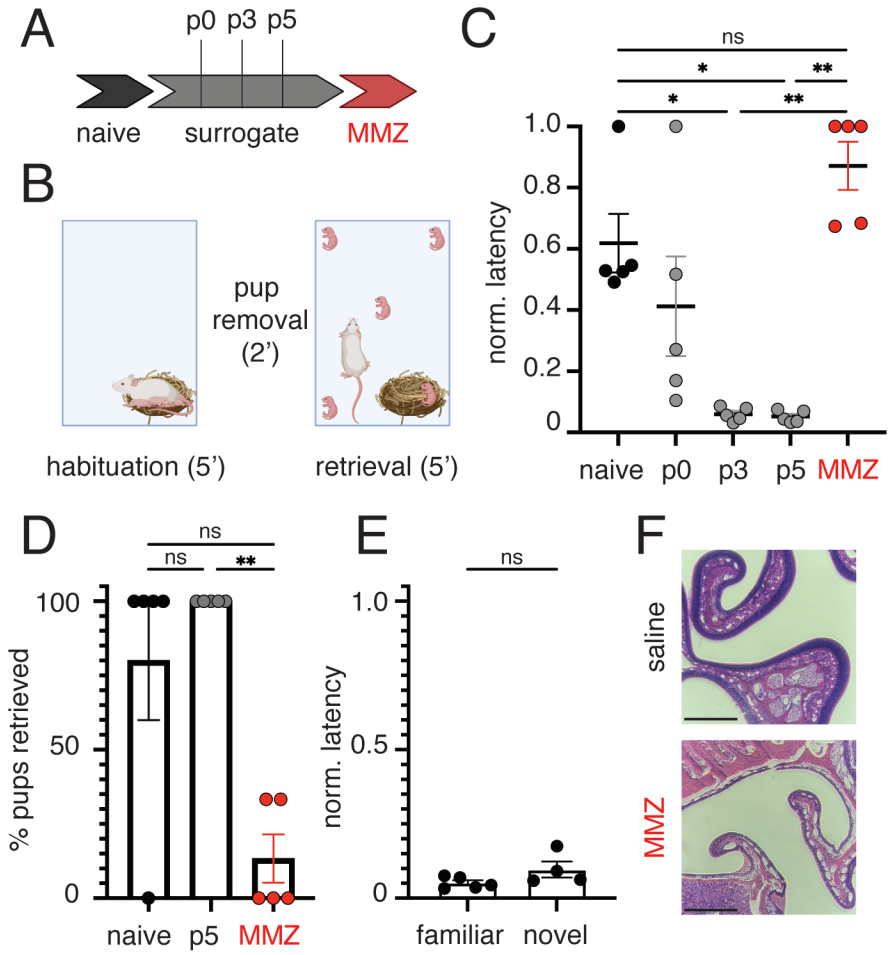

Figure 1

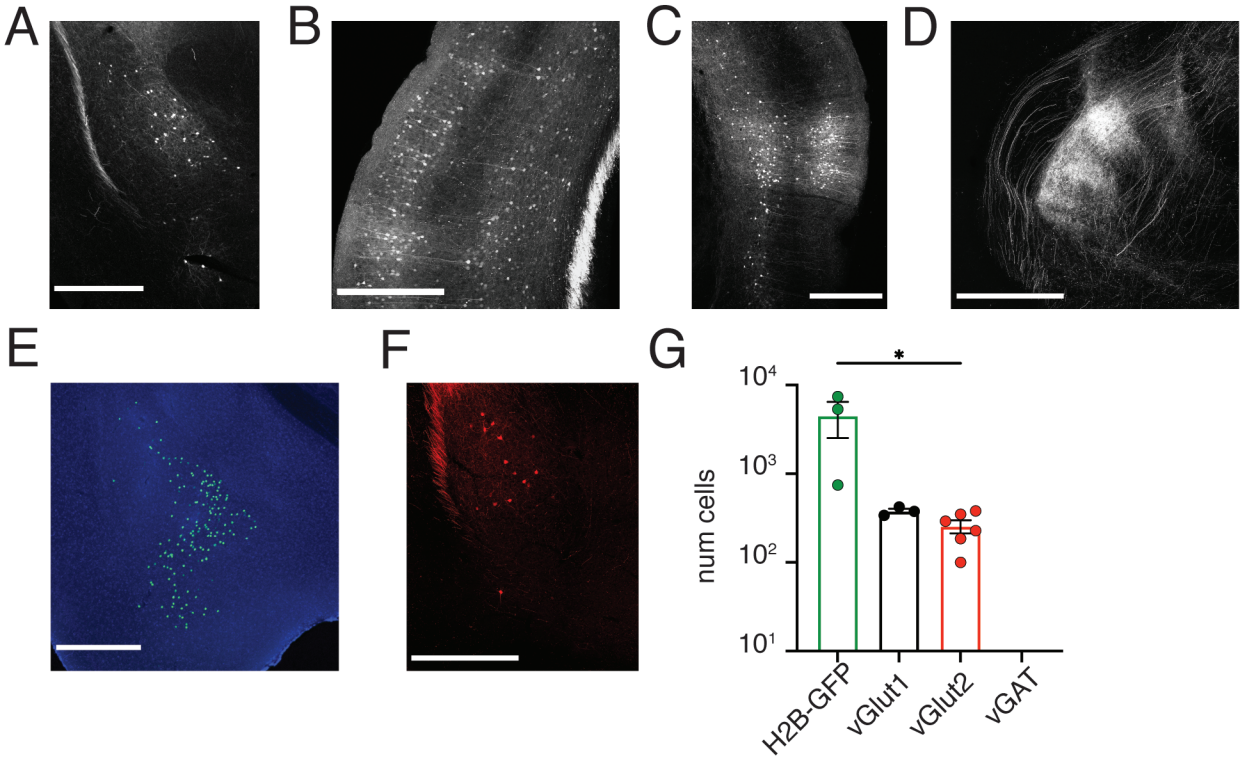

Figure 2

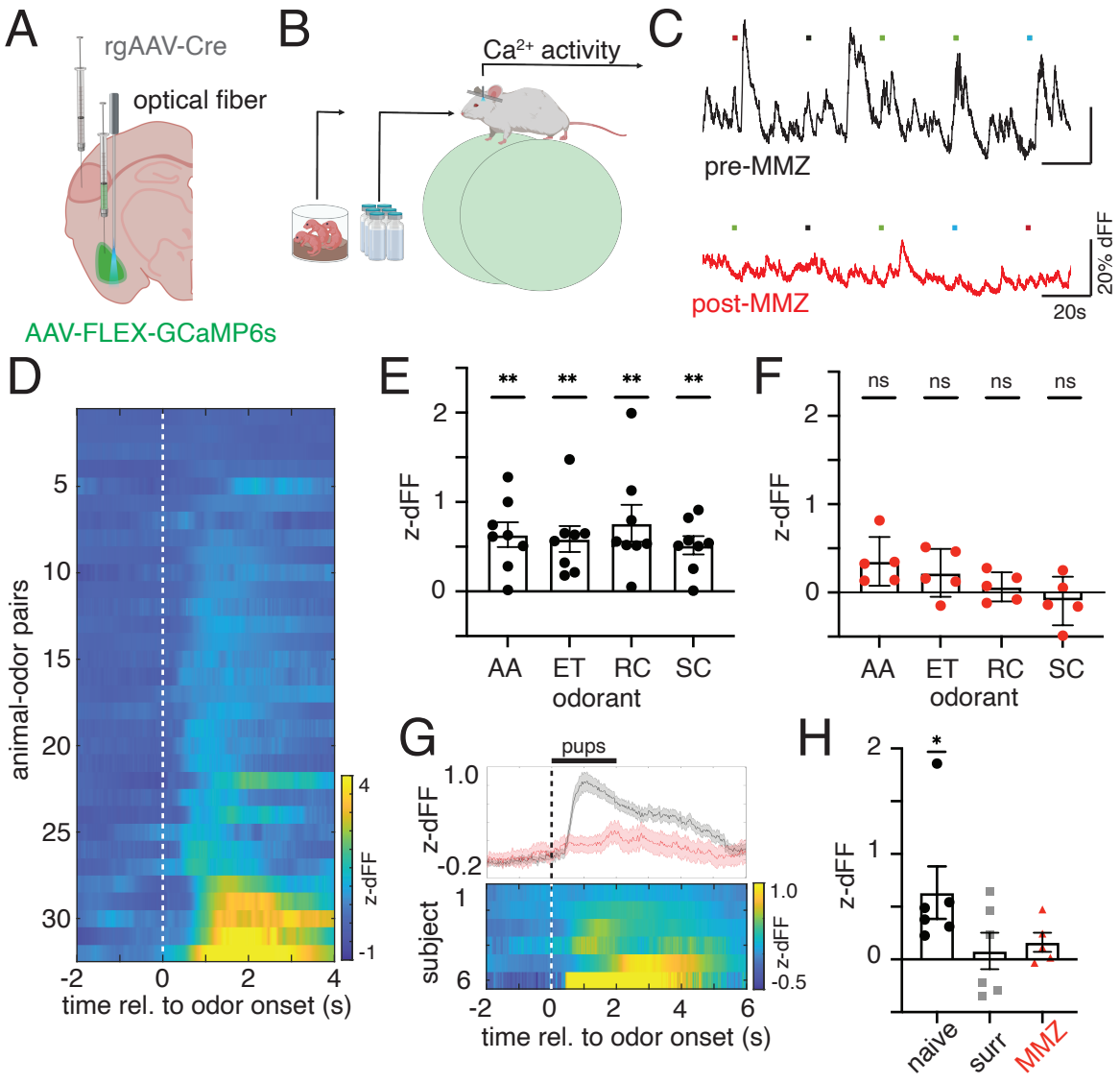

Figure 3

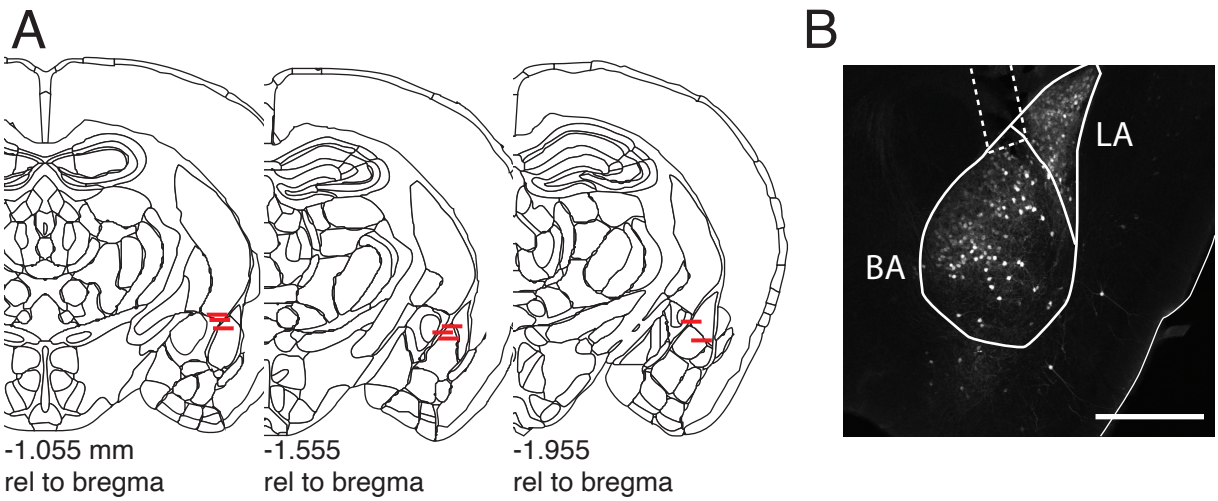

Figure 3-1

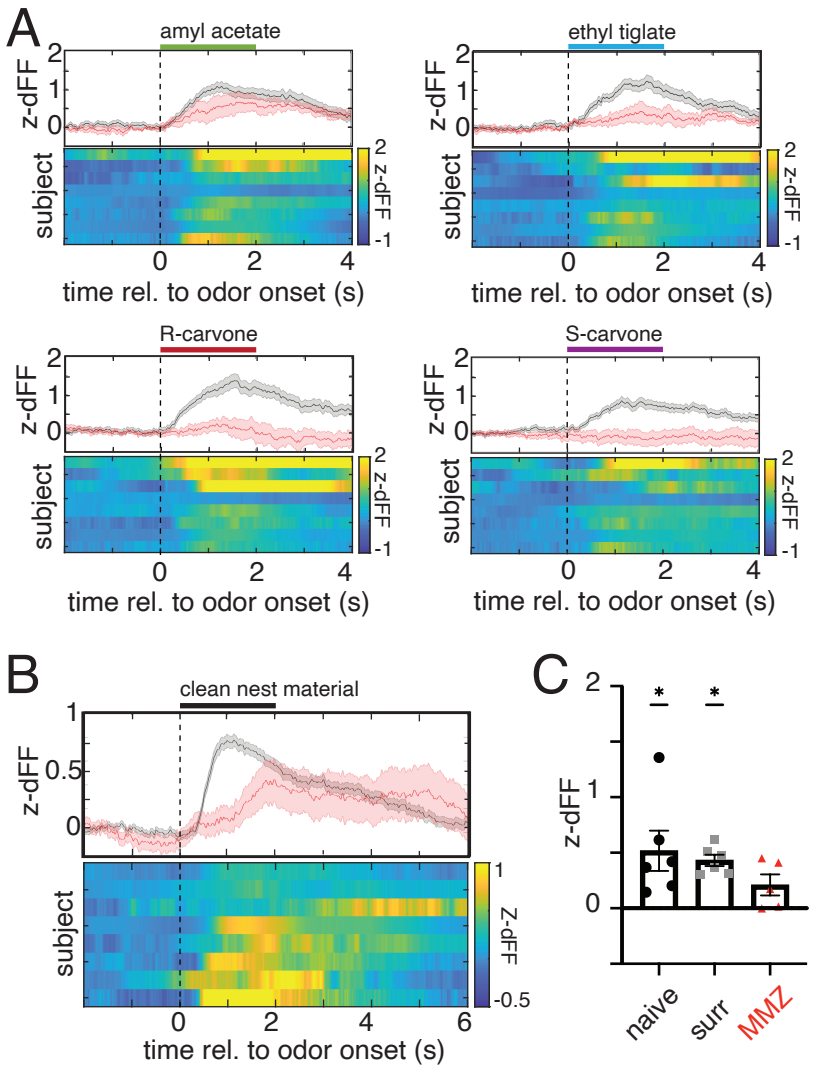

Figure 3-2

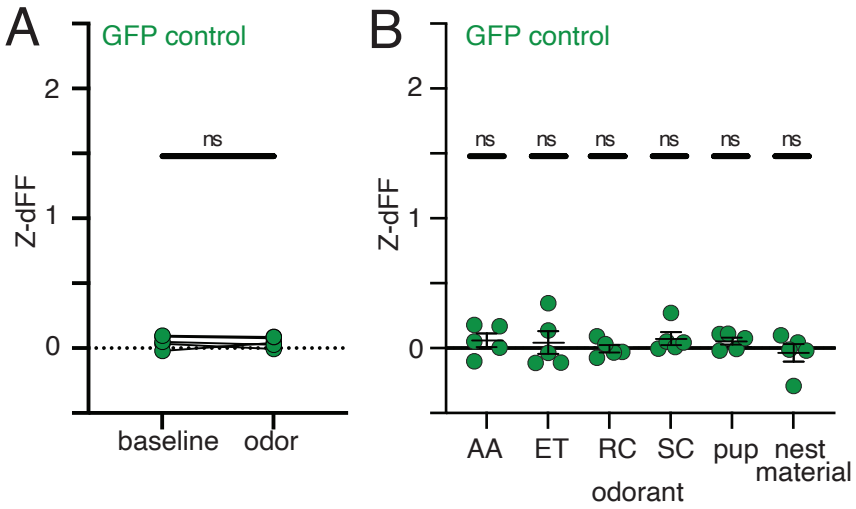

Figure 3-3

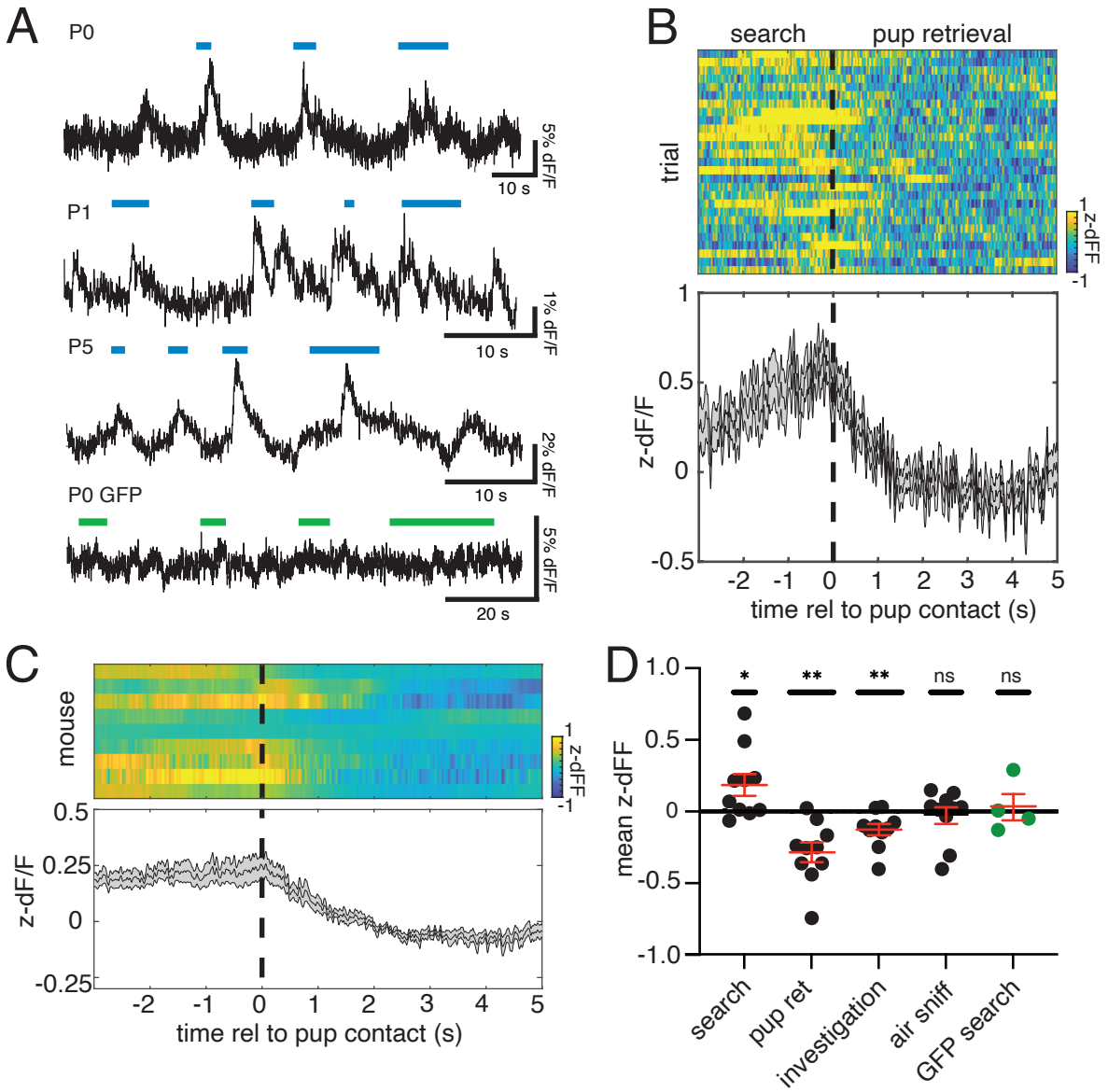

Figure 4

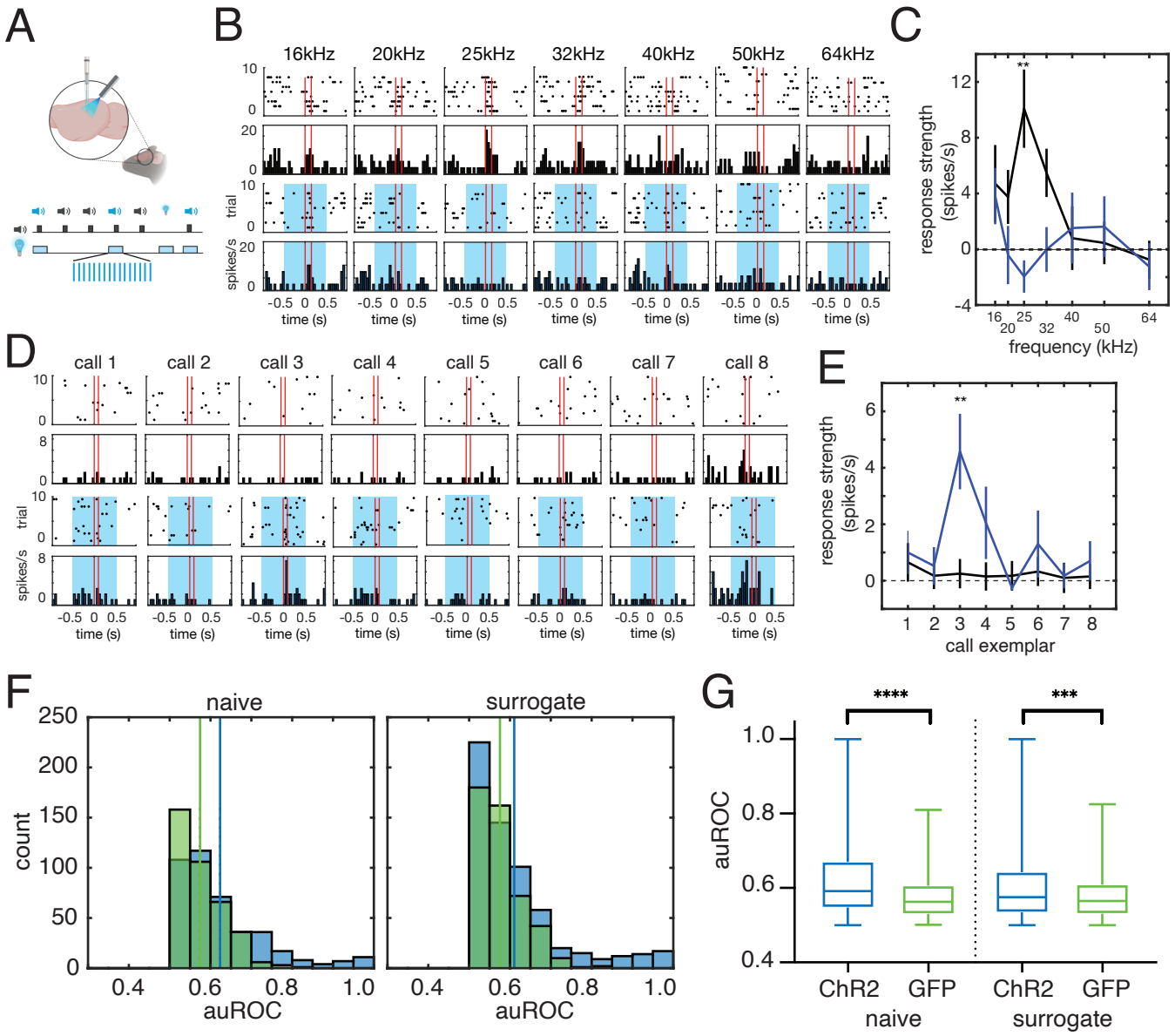

Figure 5

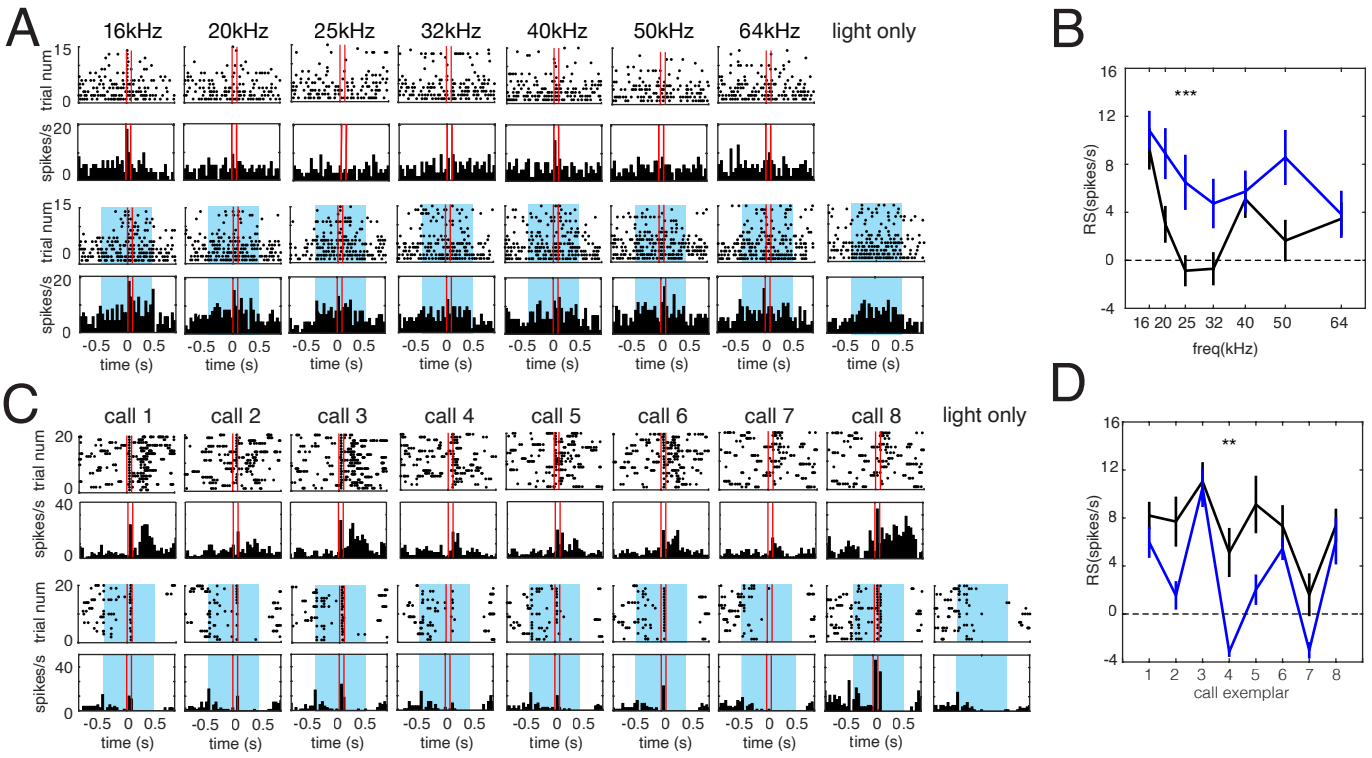

Figure 5-1

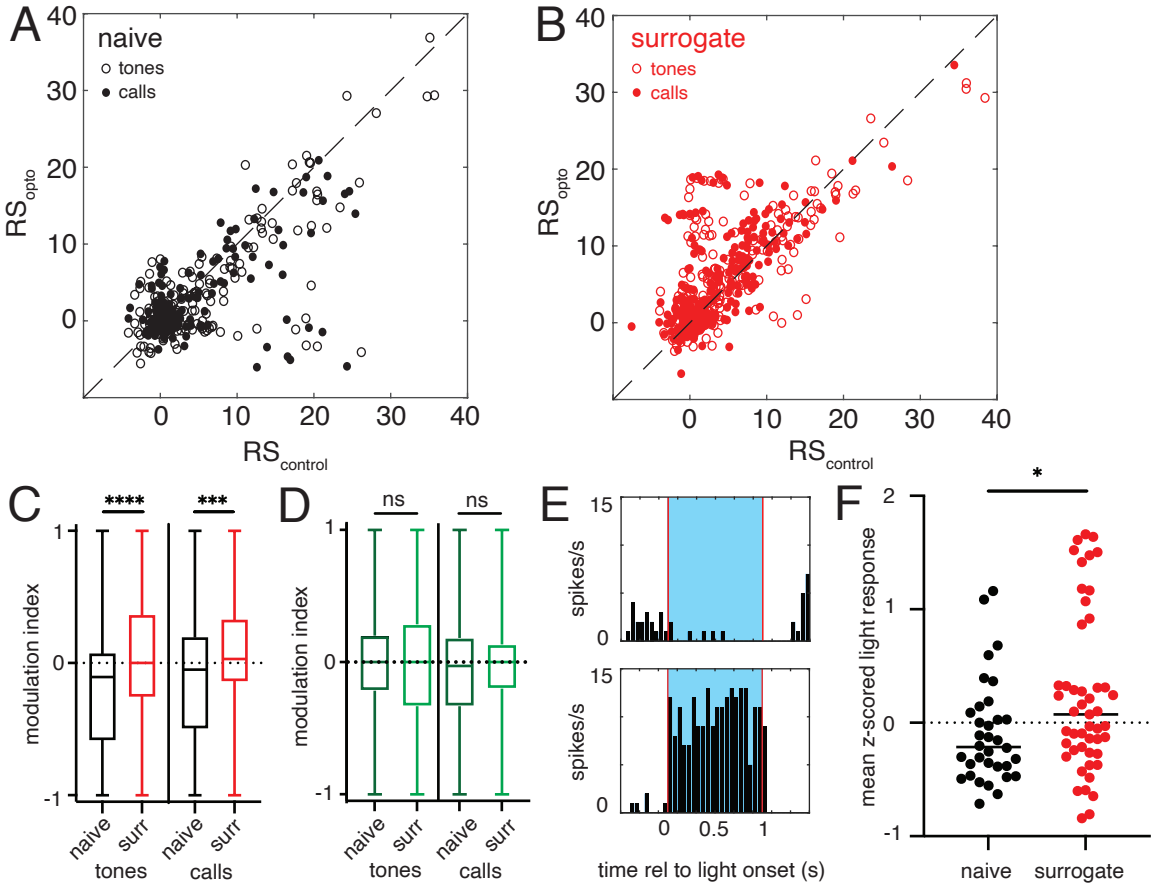

Figure 6

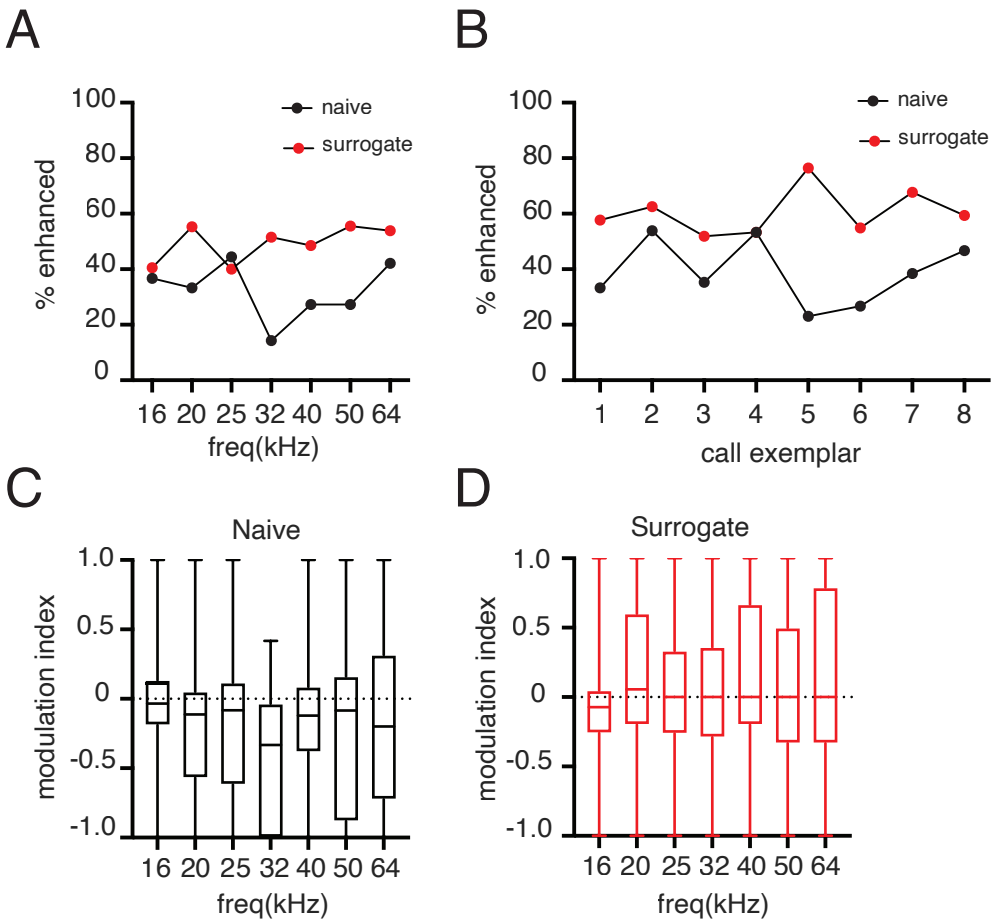

Figure 6-1